Src- and confinement-dependent FAK activation causes E-cadherin relaxation and β-catenin activity

Charlène Gayrard, Clément Bernaudin, Théophile Déjardin, Cynthia Seiler, Nicolas Borghi

JCB

Article

Src- and confinement-dependent FAK activation causes E-cadherin relaxation and β-catenin activity

Charlène Gayrard, Clément Bernaudin, Théophile Déjardin, Cynthia Seiler, and Nicolas Borghi

Institut Jacques Monod, Unité Mixte de Recherche 7592, Centre National de la Recherche Scientifique, Université Paris-Diderot, Paris, France

In epithelia, E-cadherin cytoplasmic tail is under cytoskeleton-generated tension via a link that contains β-catenin. A cotranscription factor, β-catenin, is also active in morphogenetic processes associated with epithelial-to-mesenchymal transition. β-Catenin signaling appears mechanically inducible and was proposed to follow phosphorylation-induced β-catenin release from E-cadherin. Evidence for this mechanism is lacking, and whether E-cadherin tension is involved is unknown. To test this, we combined quantitative fluorescence microscopies with genetic and pharmacological perturbations of epithelial-to-mesenchymal transition–induced cells in culture. We showed that β-catenin nuclear activity follows a substantial release from the membrane specific to migrating cells and requires multicellular deconfinement and Src activity. Selective nuclear translocation occurs downstream of focal adhesion kinase activation, which targets E-cadherin tension relaxation through actomyosin remodeling. In contrast, phosphorylations of the cadherin/catenin complex are not substantially required. These data demonstrate that E-cadherin acts as a sensor of intracellular mechanics in a crosstalk with cell-substrate adhesions that target β-catenin signaling.

Introduction

In multicellular organisms, cells generate and experience mechanical forces that may convert into biochemical signals. This process assumes that force-induced conformation changes in proteins alter their affinities, and thus their activities (Sawada et al., 2006), triggering signaling pathways that ultimately lead to changes in cell activity and fate.

In a simple epithelium, cells form tissue sheets by directly adhering to one another through adherens junctions (Borghi and Nelson, 2009). The adherens junction E-cadherin is a transmembrane protein whose extracellular domain forms intercellular dimers between adjacent cells. Its cytoplasmic tail provides mechanical coupling between the plasma membrane and the cortical cytoskeleton (Tabdanov et al., 2009) and is under constitutive cytoskeleton-generated tension sensitive to extracellular cues (Borghi et al., 2012; Rolland et al., 2014). Any biochemical events downstream of these tension changes are unknown.

A direct interaction between the E-cadherin tail and β-catenin is obligatory to tether adherens junctions to the actin cytoskeleton via α-catenin (Buckley et al., 2014), but β-catenin is also a transcription cofactor well known as an effector of Wnt, which down-regulates β-catenin degradation (Clevers and Nusse, 2012). E-cadherin is also a regulator of β-catenin signaling, in a fashion independent of, yet synergistic with, Wnt (Nelson and Nusse, 2004; Benham-Pyle et al., 2016). E-cadherin may regulate β-catenin transcriptional activity by sequestering it out of the nucleus (Sanson et al., 1996; Orsulic et al., 1999), but the mechanisms are more complex than mere modulation of E-cadherin tail levels, because β-catenin nuclear activity appears to also require E-cadherin expression (Howard et al., 2011), and its extracellular domain in particular (Benham-Pyle et al., 2015). However, there is no evidence that nuclear β-catenin actually originates from a previously membrane-bound pool.

β-Catenin nuclear localization and transcriptional activity appear mechanically inducible in health and disease models. This induction occurs during morphogenetic events sharing features with epithelial-to-mesenchymal transition (Farge, 2003; Hens et al., 2005; Whitehead et al., 2008; Brunet et al., 2013; Benham-Pyle et al., 2015; Fernández-Sánchez et al., 2015). Such nuclear translocation and activity generally require the activity of the Src kinase and appear to involve β-catenin tyrosine phosphorylation (Desprat et al., 2008; Whitehead et al., 2008; Brunet et al., 2013; Benham-Pyle et al., 2016) at a site targeted by Src in vitro that lowers β-catenin affinity for E-cadherin (Roura et al., 1999). Mechanical induction of β-catenin transcriptional activity might thus result from its release from E-cadherin because of a weakened interaction induced by the Src-dependent phosphorylation of β-catenin. The initial mechanotransduction events, and the implication of changes in E-cadherin molecular tension, remain unknown.

To address this, we performed live-cell fluorescence imaging of localization, activity, and tension reporters of E-cadherin, β-catenin, and selected signaling pathway components together with genetic and pharmacological perturbations in cultured epithelial cells induced to migrate by exposure to hepatocyte growth factor (HGF) or by wound healing, both known

Correspondence to Nicolas Borghi: nicolas.borghi@ijm.fr

The Rockefeller University Press
J. Cell Biol. Vol. 217 No. 3 1063–1077
https://doi.org/10.1083/jcb.201706013

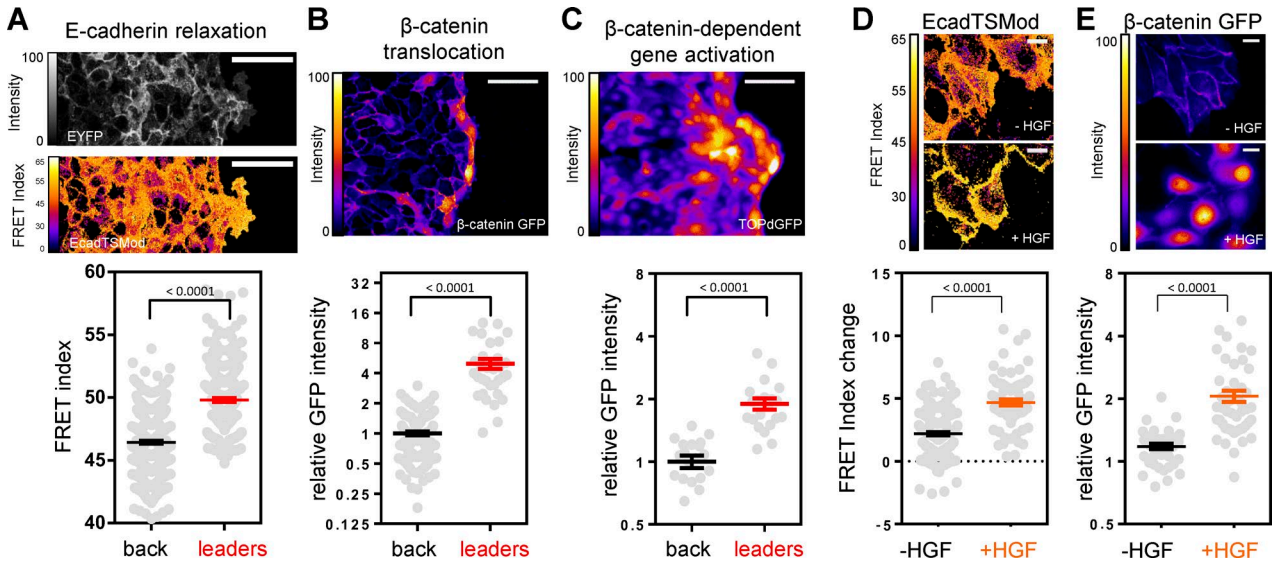

Figure 1. **E-cadherin tension relaxation correlates with β-catenin nuclear accumulation. (A)** Wounded sheet of MDCK cells expressing EcadTSMod. Top: Direct YFP fluorescence. Middle: Corresponding FRET index map. Note that this map does not display protein levels. Bottom: FRET index in leader cells lamellipodia (n = 315 cells) and cell–cell contacts at the back (~500 µm; n = 410) 10 h postwound. **(B)** GFP-β-catenin in a wounded MDCK sheet. Top: Typical map. Bottom: GFP intensity (relative to back cells) in leader cells (n = 32 cells) and cells at the back (n = 120; ~500 µm) 10 h postwound. **(C)** TOPdGFP in a wounded MDCK sheet. Top: Typical map. Bottom: GFP intensity (relative to back cells) in leader cells (n = 20 cells) and cells at the back (n = 21; ~500 µm) 10 h postwound. **(D)** FRET index of EcadTSMod in cells with and without HGF (50 ng/ml). Top: Typical maps. Bottom: FRET index change at cell–cell contacts 5 h after HGF addition (n = 72 cells) versus control (n = 173). **(E)** GFP-β-catenin in cells with and without HGF (50 ng/ml). Top: Typical maps. Bottom: GFP intensity in the nucleus (relative to cytoplasm) 5 h after HGF addition (n = 47 cells) versus control (n = 42). Bars: (wound healing) 100 µm; (HGF) 20 µm. Two-tailed Mann–Whitney test. Values plotted are mean ± SEM.

to induce epithelial-to-mesenchymal transition, at least partially (Thiery and Sleeman, 2006).

Results

E-Cadherin tension relaxation correlates with selective β-catenin nuclear accumulation and activity

In wound healing assays, normal epithelial MDCK cells migrated collectively, some exhibiting the characteristic leader phenotype with large lamellipodia at the wound edge (Omelchenko et al., 2003). Using cells expressing the E-cadherin tension fluorescence resonance energy transfer (FRET) biosensor EcadTSMod, which predominantly localized at the membrane and was enriched at cell–cell contacts as the endogenous protein (Borghi et al., 2012; Fig. 1 A), we measured FRET exclusively at cell–cell contacts in all cells (Fig. S1 A), plus at the lamellipodia in leader cells only, as we have previously shown that E-cadherin may be under tension at the membrane whether or not at cell–cell contacts (Borghi et al., 2012). We uncovered a gradient of FRET index, with FRET decreasing from leader cells lamellipodia to cell–cell contacts hundreds of micrometers back, indicative of a gradient of E-cadherin tension from low in leader cells to high in the back (Fig. S1 B). Significantly, leader cells exhibited a higher FRET than follower cells hundreds of micrometers back (Fig. 1 A), whereas no such difference could be observed in cells that expressed an E-cadherin tensionless control, which lacks its C-terminal catenin-binding and actin-recruiting part (EcadTSModΔCyto; Borghi et al., 2012; Fig. S1, C and D). FRET increased in the first hours of migration, followed by a plateau and a decrease upon contact of opposing migrating sheets, such that the confluent sheet would recover its homogenous FRET value before wounding (Fig. S1 E). Note that the total amount of E-cadherins in the EcadTSMod cell line was ~1.5 times that in the parent MDCK cell line (Fig. S1 F), an increase well below the EcadTSMod expression level differences observed in transiently transfected cells to yield overexpression artifacts visible on FRET (Borghi et al., 2012). Altogether, these results indicate that wound-induced collective migration leads to spatially graded, reversible relaxation of cytoskeleton-dependent E-cadherin tension, with lower E-cadherin tension in leader cells than in followers.

Next, we sought to assess the localization of β-catenin. Cells stably expressing β-catenin-GFP exhibited total β-catenin levels statistically indistinguishable from those in the parent cell line, associated with a significant decrease of endogenous β-catenin expression (Fig. S1 G). β-Catenin-GFP localized at cell–cell contacts as expected and was massively enriched in the nuclei of front cells in a wounded sheet. Significantly, leader cells exhibited an up to fivefold increase in β-catenin-GFP nuclear level compared with followers at 10 h after wounding (Fig. 1 B). In contrast, stably expressed α-catenin-GFP, whose level also increased in the cytoplasm of leader cells compared with followers, appeared relatively excluded from the nucleus (Fig. S1 H). To assess whether this selective β-catenin nuclear accumulation was accompanied by an increase in its transcriptional activity, we used cells carrying the TOPdGFP sensor, which expresses destabilized GFP under the control of the LEF-1/TCF promoter (Dorsky et al., 2002; Maher et al., 2009). Significantly, leader cells expressed twice as much GFP as followers (Fig. 1 C). Altogether, these results show that wound-induced migration results in nuclear accumulation and transcriptional activity of β-catenin in leader cells, together with E-cadherin relaxation.

To assess whether such a correlation holds in other conditions, we stimulated MDCK colonies with HGF. HGF induces

MDCK scattering (de Rooij et al., 2005) and LEF-1/TCF–dependent gene expression (Howard et al., 2011), although evidence for concomitant β-catenin nuclear accumulation is unclear. Here, subconfluent MDCK colonies underwent significant cell-substrate spreading during the first 2 h after HGF exposure (Fig. S1 I). Cell–cell contact disruption progressively followed over the next hours, which ultimately resulted in mesenchymal cells migrating individually, as previously reported. In addition, EcadTSMod FRET increased at cell–cell contacts under HGF stimulation, such that HGF-stimulated cells exhibited significantly higher FRET than unstimulated cells, at times (5 h) before complete cell–cell contact disruption (Fig. 1 D). In contrast, EcadTSModΔCyto cells exhibited no such change in FRET upon HGF stimulation (Fig. S1 J). Finally, we showed that HGF induced a twofold increase in nuclear β-catenin-GFP, to a level significantly higher than that of nontreated cells (Fig. 1 E). Altogether, these results support that a correlation between E-cadherin tension relaxation and β-catenin nuclear accumulation and activity is a common feature of cells induced to migrate through various perturbations.

Membrane β-catenin substantially contributes to β-catenin nuclear accumulation

To assess the possibility of a translocation of cadherin-bound β-catenin to the nucleus, we made a cell line that stably expressed the green-to-red photoconvertible β-catenin-mMaple. Under HGF stimulation, photoconverted cell–cell contact β-catenin-mMaple translocated to the nucleus (Fig. 2 A). Quantitatively, the nuclear concentration of photoconverted β-catenin-mMaple within 5 min after photoconversion reached up to 50% of that of cell–cell contacts before photoconversion (Fig. 2, B and C). In contrast, the nuclear concentration of photoconverted β-catenin-mMaple within the same time frame reached no more than 20% of that of cell–cell contacts before photoconversion in unstimulated cells (Figs. 2 C and S2 A). In addition, during wound healing, the nuclear concentration of photoconverted β-catenin-mMaple of leader cells reached up to 60% of that of the lamellipodium before photoconversion at a rate consistent with that of a membrane-bound pool rather than that of a cytoplasmic pool (Fig. 2, C and D; and Fig. S2 B). Thus, whether at a cell–cell contact or not, β-catenin-mMaple feeds the nucleus from a membrane-bound pool. To confirm this, we measured by FRAP the entry rate of β-catenin-GFP in the lamellipodia and at cell–cell contacts of migrating cells, that of E-cadherin-GFP in the same subcellular regions, and the turnover rates of free GFP and cytoplasmic β-catenin-GFP in cells treated with LiCl, an inhibitor of the β-catenin degradation complex component GSK3β. β-Catenin-GFP entry rates in lamellipodia and cell–cell contacts of migrating cells were significantly different from that of free GFP and β-catenin-GFP in LiCl-treated cells and, together with the corresponding mobile fractions, correlated with that of membrane-bound E-cadherin instead (Fig. S2 C). This is consistent with a membrane-bound pool of β-catenin associated with E-cadherins, both in lamellipodia and at cell–cell contacts. Altogether, these results show that upon HGF- or wound-induced migration, the nuclear concentration of previously membrane-bound β-catenin reaches within minutes more than half of that of intercellular contacts, a proportion two to three times larger than without stimulation.

Besides dissociation of the E-cadherin/β-catenin complex, changes in β-catenin nuclear-to-membrane ratio (*N/M*) may in principle also result from changes in rates of β-catenin synthesis and degradation, the latter process known to occur in the cytoplasm as well as at the membrane (Maher et al., 2009), or mere changes in E-cadherin levels, although not likely to occur under HGF stimulation within the timeframe of our experiments (Weidner et al., 1990; de Rooij et al., 2005; Loerke et al., 2012). To account for these possibilities, we built a phenomenological, three-reservoir model of β-catenin level homeostasis in which a cytoplasmically synthesized β-catenin pool can exchange with membrane and nuclear pools and be degraded in all three pools independently (Fig. S2 D). We found that changes, if any, in membrane pool capacity, degradation, or synthesis rates affected *N/M* only if degradation rates were significant compared with apparent exchange rates or membrane pool saturation was reached (Fig. S2 D).

To test these possibilities, we first measured β-catenin degradation rates by following the decay of whole-cell, photoconverted β-catenin-mMaple. Regardless of whether cells were under HGF stimulation, leader, or follower cells, the half-life of β-catenin-mMaple was around several hours (Fig. S2 E), much longer than the membrane entry and exit half-times of β-catenin in migrating cells (Fig. S2, B and C). In addition, its dependence on HGF exposure and cell position in the migrating sheet was inconsistent with a role in β-catenin nuclear accumulation: cells away from a wound edge exhibited the slowest β-catenin degradation rate (Fig. S2 E) while having shown no β-catenin nuclear accumulation (Fig. 1 B). Moreover, we did not observe differential decay between compartments, which, unless compartment-specific degradation rates are all equal, implies that apparent exchange rates are higher, consistently with exchange rates measured earlier (Fig. 2 B and Fig. S2, B and C). To fully confirm this, we measured β-catenin-mMaple exit and β-catenin-GFP entry rates in the membrane pool, with or without HGF. All apparent exchange rates were within the minute timescale (Fig. S2, F and G), where the nucleus exchange rates were also previously found (Krieghoff et al., 2006). Altogether, these results show that degradation rates are too slow and their changes too small to account for an increase in β-catenin *N/M* in migration-induced cells.

If the β-catenin membrane pool was saturated, *N/M* could in principle change also as a result of changes in synthesis rates or membrane pool capacity (Fig. S2 D). We thus monitored by whole-cell FRAP β-catenin-GFP synthesis, which may undergo endogenous translational regulation (Song et al., 2015). Times required to recover pre-FRAP β-catenin-GFP levels exceeded 5 h and were insensitive to HGF stimulation (Fig. S2 H). Finally, we assessed total E-cadherin-GFP levels and found no decrease up to at least 10 h after HGF stimulation (Fig. S2 I). Altogether, these results show that if the β-catenin membrane pool was saturated, this could nevertheless not account for changes in β-catenin nuclear accumulation in migrating cells.

Finally, we sought to assess whether β-catenin translocation from the membrane was not merely a generic process occurring whenever β-catenin accumulates in the nucleus. We thus monitored β-catenin-mMaple membrane-to-nucleus transport in cells exposed to LiCl (Fig. 2 E). The nuclear concentration of photoconverted membrane-bound β-catenin-mMaple was not significantly different from that in untreated cells 5 min after photoconversion (30%), in contrast to that in HGF-treated or leader cells (Fig. 2, B and C). Moreover, LiCl-treated cells experienced no E-cadherin tension relaxation (Fig. 2 F). This result further supports that β-catenin membrane-to-nucleus translocation is

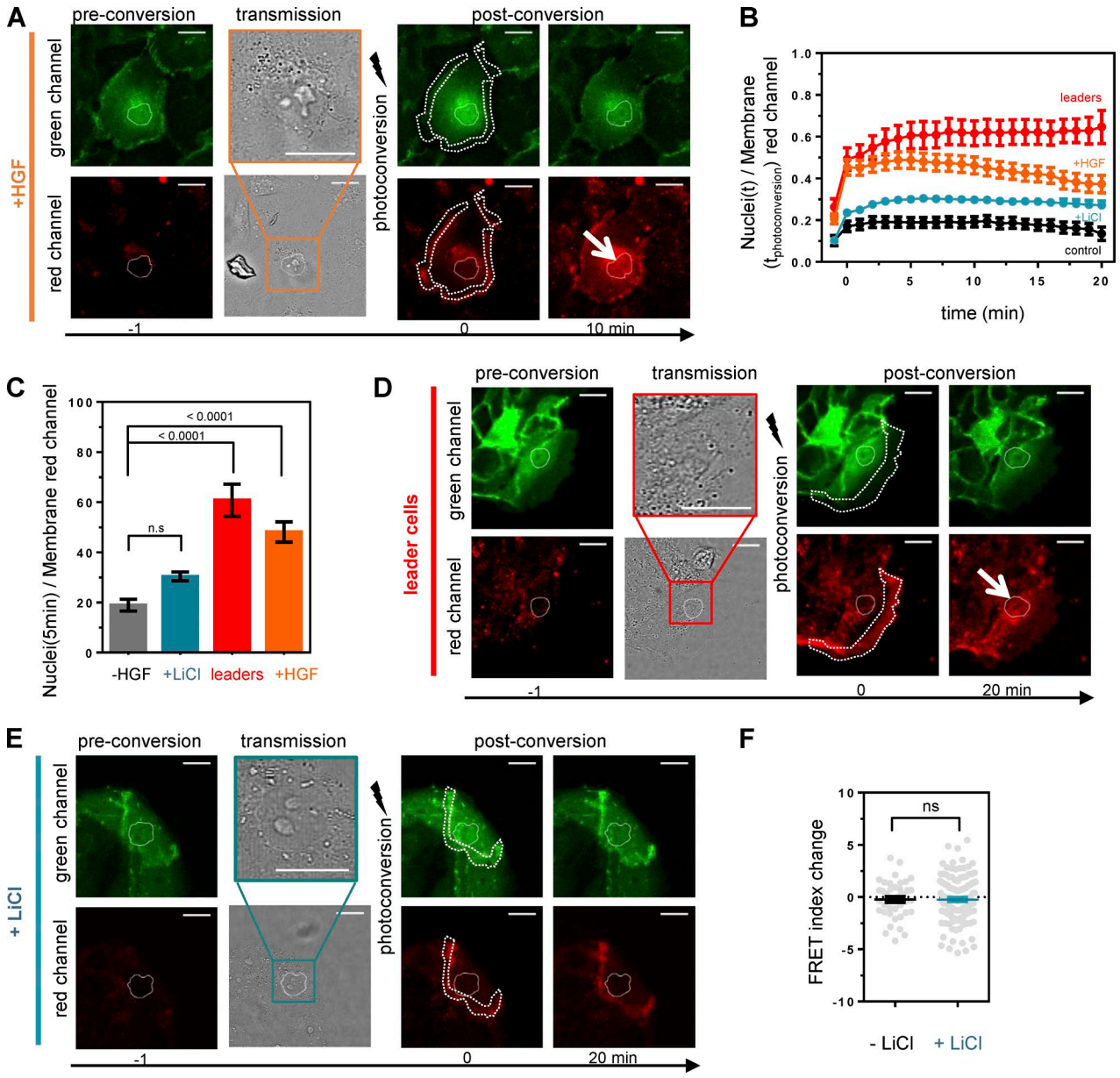

Figure 2. **Nuclear β-catenin significantly comes from the membrane. (A)** Localization of photoconvertible mMaple-β-catenin through time in cells 4 h after HGF. **(B)** Photoconverted mMaple-β-catenin in the nucleus through time (red intensity in the nucleus at *t* relative to red intensity in photoconverted region at *t* = 0 s) for leader cells in a wound (*n* = 18 cells), cells 4 h after HGF (*n* = 23 cells), unstimulated cells (*n* = 14), and 5 h post-LiCl (*n* = 37). **(C)** Photoconverted mMaple-β-catenin red intensity in the nucleus at 5 min relative to red intensity in photoconverted region at *t* = 0 s for leader cells in a wound (*n* = 18 cells), cells 4 h after HGF (*n* = 23), unstimulated cells (*n* = 14), and 5 h post-LiCl (*n* = 37). **(D)** Localization of photoconvertible mMaple-β-catenin through time in leader cells of a wounded sheet. **(E)** Localization of photoconvertible mMaple-β-catenin through time in cells 5 h post-LiCl (30 mM). **(F)** FRET Index change of EcadTSMod in MDCK cells after 5 h of LiCl stimulation (30 mM; *n* = −/+ 41/132 cells). Bars, 20 µm. Solid line indicates the nuclei based on transmission image. Dotted line indicates region of 405-nm photoconversion at *t* = 0 s. White arrow shows nuclear accumulation of photoconverted mMaple-β-catenin within minutes. Two-tailed Mann–Whitney or Kruskal–Wallis tests. Values plotted are mean ± SEM. ns, not significant.

concomitant with E-cadherin relaxation and shows in addition that E-cadherin relaxation is not a consequence of β-catenin nuclear accumulation or of any of its subsequent effects.

Altogether, these results show that specifically in migration-induced cells, β-catenin nuclear accumulation is a consequence of a substantial β-catenin release from the membrane that is concomitant with E-cadherin relaxation and cannot be explained by changes in synthesis, degradation, or membrane pool capacity. Instead, a change in E-cadherin/β-catenin affinity may explain the results.

E-cadherin relaxation and β-catenin translocation are non-cell autonomous through a cell confinement release mechanism

That E-cadherin relaxed at and β-catenin translocated from both intercellular contacts and contact-free regions raised the question whether these processes were cell autonomous. To test this, we examined β-catenin localization and E-cadherin tension in individual cells exposed to HGF (Fig. 3 A). In those cells, β-catenin did not translocate to the nucleus and E-cadherin did

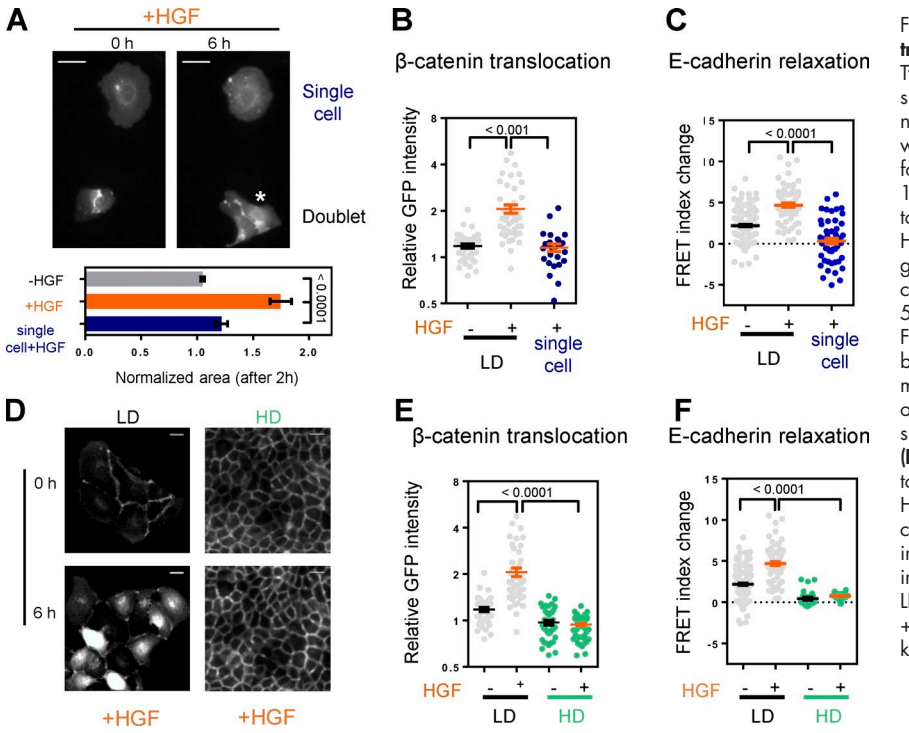

Figure 3. **E-cadherin relaxation and β-catenin translocation are non–cell autonomous. (A)** Top: Typical micrographs of GFP-β-catenin cells either single or doublet cells with or without HGF (50 ng/µL). Bottom: Normalized area of cells with or without HGF (data from Fig. S1 I) after 2 h and for single cells after 2 h of HGF treatment (n = 10 cells). **(B)** GFP intensity in the nucleus (relative to cytoplasm) of GFP-β-catenin 5 h with or without HGF (50 ng/ml; data from Fig. 1 E) and for single cells under HGF (n = 26 cells). **(C)** FRET index change at cell–cell contacts of EcadTSMod cells 5 h with and without HGF (50 ng/ml; data from Fig. 1 D), and for single cells at the basal membrane 5 h with HGF (n = 53 cells). **(D)** Typical micrographs of GFP-β-catenin cells with and without HGF (50 ng/ml) for island of cells at low density (LD) and confluent cells at high density (HD). **(E)** GFP intensity in the nucleus (relative to cytoplasm) of GFP-β-catenin 5 h with or without HGF (50 ng/ml) at LD (data from Fig. 1 E), and confluence (HD; n = −/+ 75/40 cells). **(F)** FRET index change at cell–cell contacts of EcadTSMod in cells 5 h with and without HGF (50 ng/ml) at LD (data from Fig. 1 D) and confluence (HD; n = +/− 27/30 cells). Bars, 20 µm. Two-tailed Kruskal–Wallis test. Values plotted are mean ± SEM.

not relax upon HGF exposure (Fig. 3, B and C). Thus, these processes are non–cell autonomous.

Moreover, we noticed that individual cells did not exhibit increased spreading on the substrate upon HGF exposure (Fig. 3 A), although their areas before stimulation were visibly larger than that of cells in subconfluent colonies (Fig. 3 A). Thus, we speculated that cell spreading was associated with E-cadherin relaxation and β-catenin translocation, and that cells controlled each other through mere confinement. Indeed, wound healing assays show consistently that unconfined leader cells exhibited relaxed E-cadherin and nuclear β-catenin, whereas confined cells in the back did not (Fig. 1). To directly test that the release of cell confinement from neighbor cells was required, we monitored β-catenin localization and E-cadherin tension in cells exposed to HGF at confluence, unable to escape confinement (Fig. 3 D). In those cells, confluence prevented both β-catenin translocation and E-cadherin relaxation (Fig. 3, F and E).

Altogether, these results support that E-cadherin relaxation and β-catenin translocation require a non–cell-autonomous release of cell confinement that allows cell-substrate spreading. We next sought to determine the molecular players involved.

E-cadherin relaxation and β-catenin translocation require Src family kinase activity independently of E-cadherin or β-catenin phosphorylations

In several model systems, mechanically induced β-catenin nuclear localization and activity permissively require the kinase Src (Desprat et al., 2008; Whitehead et al., 2008; Brunet et al., 2013; Benham-Pyle et al., 2016). Src can induce tyrosine phosphorylation of β-catenin in vitro, which lowers the affinity of β-catenin for E-cadherin (Roura et al., 1999), and is widely assumed to suffice for the complex dissociation in situ.

We assessed Src activity requirement with its inhibitor PP1. On HGF-treated MDCK colonies, Src inhibition was accompanied by an arrest in cell spreading, scattering, and β-catenin-GFP nuclear accumulation (Fig. 4, A and B). The inhibition also resulted in a prominent and severe impairment of E-cadTSMod tension relaxation (Fig. 4 C), supporting a Src activity upstream of cell spreading and both β-catenin translocation and E-cadherin relaxation. To confirm this, we treated cells undergoing wound healing with PP1. Src inhibition was associated with a dramatic decrease in sheet migration velocity, as expected (Matsubayashi et al., 2004), and leader cell numbers (Fig. 4 D). In addition, the inhibition also led to a significant drop in β-catenin-GFP nuclear translocation and impaired EcadTSMod tension relaxation in front (for lack of leader) cells (Fig. 4, E and F).

We next sought to assess whether Src activity was constitutive with an adapted FRET-based sensor of Src kinase activity (Wang et al., 2005; Fig. S3 A). Upon cell exposure to HGF, the stably expressed Src sensor exhibited no decrease in FRET (Fig. S3 B). In contrast, coexpression with an mCherry-tagged constitutively active form of Src (Y527F) led to FRET decrease, confirming the sensor sensitivity. Conversely, addition of PP1 increased FRET, as expected for an inhibition of Src activity. These results confirm that Src activity is constitutive and are consistent with its requirement for β-catenin nuclear translocation, but also E-cadherin relaxation.

Next, we sought to assess whether β-catenin was the relevant Src target. We generated cell lines that stably expressed β-catenin-GFP phospho mutants Y654E or Y654F, which have affinities for E-cadherin lower than that of Src-phosphorylated β-catenin and equal to that of unphosphorylated β-catenin, respectively (Roura et al., 1999). In cell colonies, the Y654F mutant exhibited a predominant membrane localization as expected, but the Y654E did as well (Fig. 4 G). Under HGF stimulation, both mutants exhibited a significant increase in nuclear localization, as WT β-catenin did (Fig. 4, G and H). These results show that β-catenin 654-tyrosine-phosphorylation is neither necessary nor sufficient for substantial nuclear translocation in migration-induced cells. Nevertheless, nuclear

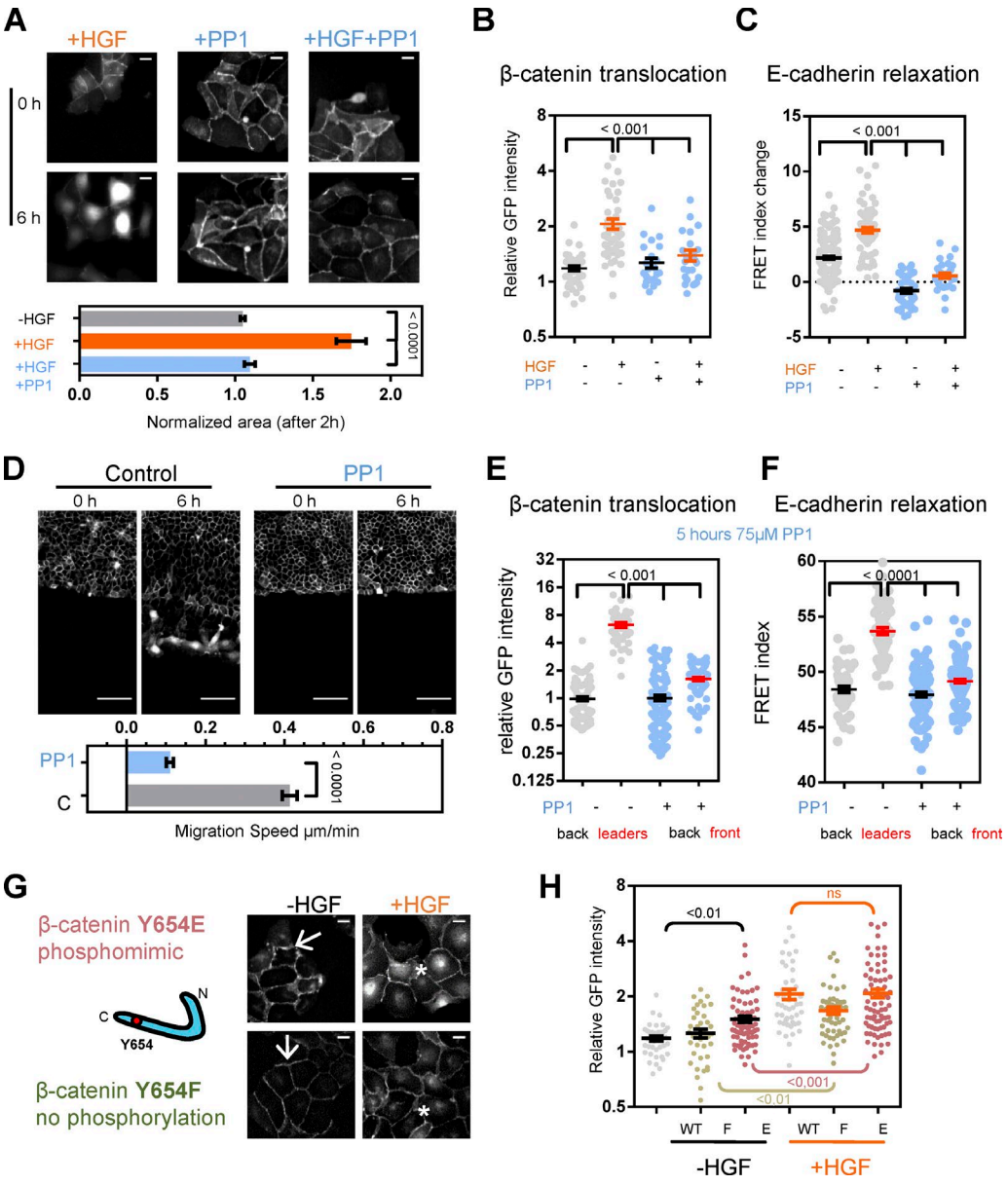

Figure 4. **Src activity is required and constitutive, but targets are not in the E-cadherin/β-catenin complex. (A)** Top: Typical micrographs of GFP-β-catenin cells with and without HGF and PP1. Bottom: Area after 2 h normalized by the area at $t = 0$ for unstimulated cells ($n = 5$ cells), HGF ($n = 15$; data from Fig. S1 I), and HGF- and PP1-treated ($n = 9$) cells. **(B)** GFP intensity in the nucleus (relative to cytoplasm) of GFP-β-catenin 5 h with or without HGF (50 ng/ml; data from Fig. 1 E), and with PP1 (25 µM) with and without HGF ($n = +/- 24/25$ cells). **(C)** FRET index change at cell–cell contacts of EcadTSMod in cells 5 h with and without HGF (50 ng/ml; data from Fig. 1 D), and with PP1 (25 µM) with and without HGF ($n = +/- 29/43$ cells). **(D)** Top: Typical micrographs of wounded sheet migration of GFP-β-catenin cells with and without PP1 (75 µM). Bottom: Migration speed (mean distance traveled by cell front per hour) with or without PP1 (75 µM; $n = -/+ 107/117$ cells). **(E)** GFP intensity in the nucleus (relative to cytoplasm) of GFP-β-catenin in leader and back cells 5 h postwound, with or without PP1 (75 µM; n = leaders $-/+ 43/69$, back $-/+ 116/114$ cells). **(F)** FRET index of EcadTSMod cells in leader lamellipodia and cell–cell contact at the back 5 h postwound, with or without PP1 (75 µM; n = leaders $-/+ 68/122$, back $-/+ 49/104$ cells). **(G)** Localization of GFP-β-catenin Y654E or Y654F in cells with and without HGF. Arrows show membrane localization of both mutants in unstimulated cells and nuclear localization of both mutants in HGF-treated cells. **(H)** GFP intensity in the nucleus (relative to cytoplasm) of GFP-β-catenin WT (data from Fig 1 E) and Y654F and E mutants in cells 5 h with or without HGF (n = F: $-/+ 40/52$, E: $-/+ 77/77$ cells). Bars: (wound healing) 100 µm; (HGF) 20 µm. Two-tailed Mann–Whitney or Kruskal–Wallis tests. Values plotted are mean ± SEM. ns, not significant.

levels of Y654E and Y654F mutants suggest that β-catenin tyrosine phosphorylation may marginally contribute to nuclear translocation (Fig. 4 H).

We thus sought another Src target. Up-regulation of Src activity results in E-cadherin phosphorylation of Y754-755-756 (Fujita et al., 2002), and Src-phosphorylated E-cadherin has a lower affinity for β-catenin (Catimel et al., 2006). Moreover, Y754-755-756 phosphorylations favor E-cadherin binding to the ubiquitinase Hakai at the expense of p120, which is thought to promote E-cadherin endocytosis (Ishiyama et al., 2010). Indeed, Y-to-F mutations in 754 to 756 prevent Hakai binding (Mukherjee et al., 2012). Consistently with impaired endocytosis, the triple phospho-impaired E-cadherin-FFF-GFP exhibited a lower mobile fraction than its WT counterpart (Fig. S3 C). Conversely, the phosphomimetic mutant E-cadherin-EEE-GFP exhibited a slightly higher mobile fraction (Fig. S3 C). To test

whether these phospho-dependent affinity and endocytic mechanisms may lead to E-cadherin tension relaxation, we generated a cell line that stably expressed the triple phospho-impaired mutant EcadTSMod-FFF (Fig. S3 D). Upon HGF stimulation, colonies of those cells exhibited a significant FRET increase compared with unstimulated colonies (Fig. S3 E). Consistently, leader cells exhibited a higher FRET than followers in a wound healing assay (Fig. S3 E). Both FRET increases were in magnitude comparable to that of EcadTSMod in the same conditions (Fig. 1). These results show that neither a change in E-cadherin/β-catenin affinity nor endocytosis caused by Y754-755-756 phosphorylations is required for E-cadherin relaxation. Altogether, these results show that Src-dependent phosphorylations of β-catenin or E-cadherin involved in the complex affinity or its endocytosis are not the major causes of E-cadherin relaxation and β-catenin translocation in migration-induced cells.

E-cadherin relaxation and β-catenin translocation require Src activation of FAK

We sought to localize Src activity in migration-induced cells away from the cadherin/catenin complex. Because conditional overexpression of Src recapitulates HGF-induced epithelial cell scattering (Behrens et al., 1993), we used SrcY527F, which promoted membrane protrusions in transiently transfected cells, as expected (Fig. S4 A). In addition, EcadTSMod exhibited a higher FRET in SrcY527F-positive cells than in nontransfected cells (Fig. S4, A and B), and SrcY527F-expressing cells showed a twofold increase of nuclear β-catenin-GFP compared with nontransfected cells (Fig. S4, A and C). Moreover, Src Y527F also localized at focal adhesions in those protrusions (Fig. S4 D), as previously seen in cancer cells (Avizienyte et al., 2002). These results show that Src activity above endogenous levels can bypass a wound- or HGF-induced E-cadherin relaxation and β-catenin translocation, and suggest that this is a consequence of Src activity at focal adhesions. FAK is a Src substrate (Calalb et al., 1995) involved in the regulation of cell migration and cell–cell adhesion (Schaller, 2010). FAK phosphorylation is also required to impair E-cadherin recruitment to cell–cell contacts upon exogenous expression of constitutively active Src in cancer cells (Avizienyte et al., 2002). FAK may thus be the Src target responsible for E-cadherin relaxation and β-catenin translocation in migration-induced normal epithelial cells.

Under HGF treatment, cells stably expressing an adapted FRET-based sensor of FAK activity (Seong et al., 2011) exhibited lower FRET than nonstimulated cells (Fig. 5, A and B), revealing that HGF increased FAK activity, in contrast with the steady activity of Src in the same conditions. In addition, pharmacological inhibition of FAK by PF228 increased FRET compared with nontreated cells, as expected, as did Src family kinases inhibition by PP1 (Fig. 5 B). Because E-cadherin relaxation and β-catenin translocation appeared concomitant with non-cell autonomous cell spreading (Fig. 3), we assessed FAK activity in isolated cells upon HGF exposure. FAK activity was insensitive to HGF addition in isolated cells, just like E-cadherin tension and β-catenin localization (Fig. 5 B). This shows that FAK activation is non–cell autonomous too. Thus, we directly assessed whether FAK activation required multicellular deconfinement and found that FAK activation by HGF was impaired by confluence (Fig. 5 B). Altogether, these results support that multicellular deconfinement and Src constitutive activity are required for FAK activation and are consistent with a role of FAK upstream of E-cadherin tension and β-catenin localization.

To confirm FAK activation, we monitored FAK tyrosine-phosphorylation by Western blot of whole-cell lysates. FAK contains Y397, which is the target of FAK itself and is involved in a Src interaction when phosphorylated, and Y576/577 and Y861, which are Src targets and prevent FAK autoinhibition by its FERM domain when phosphorylated (Lietha et al., 2007; Fig. 5 C). Under HGF stimulation, Y397 and Y576/577 phosphorylations increased compared with untreated cells (Fig. 5, C and D). Consistently, inhibition by PF228 in HGF-treated cells resulted in a decrease in all phosphorylations to levels below that of untreated cells (Fig. 5, C and D). In addition, inhibition by PP1 in HGF-treated cells decreased the phosphorylation of its targets Y576/577 and Y861 to levels below that of untreated cells, and to a lesser extent that of the FAK autophosphorylation site Y397 (Fig. 5, C and D). Altogether, these results match a model in which HGF induces some FAK autophosphorylation independently of Src, which is further enhanced by Src after its FAK binding–dependent phosphorylation of Y576/577 and Y861.

Finally, we sought to directly test the requirement of FAK activity for β-catenin translocation and E-cadherin relaxation in migration-induced cells. In HGF-treated cells, inhibition of FAK by PF228 abolished cell spreading and led to a complete impairment of β-catenin-GFP translocation and EcadTSMod FRET increase (Fig. 5, E–G), in a fashion similar to that of Src kinase inhibition (Fig. 4, A–C). In wound-induced migrating cell sheets, inhibition of FAK by PF228 severely impaired sheet migration (Fig. 5 H), in a fashion similar to that of Src inhibition (Fig. 4, D–F). Altogether, these results support that induction of cell migration activates FAK by permissive Src activity, which subsequently results in cell spreading, E-cadherin relaxation, and β-catenin translocation.

Src-FAK-dependent actomyosin remodeling is sufficient for E-cadherin relaxation, and dissociation of β-catenin is not required

Cell spreading suggests dramatic cytoskeletal remodeling, and FAK targets several regulators of the actomyosin cytoskeleton architecture and dynamics (Schaller, 2010). Thus, we sought to characterize the Src-FAK-dependent remodeling of actomyosin in migrating cells.

Cells exposed to HGF exhibited about twice as much phalloidin-stained, ventral actin stress fibers distinct from cell–cell contacts and stemming from FAK-positive focal adhesions as cells not exposed to HGF (Fig. 6, A and B; and Fig. S5 A). Exposure of HGF-treated cells to PP1 or PF228 led in both cases to a significant decrease in stress fiber number to values similar to or below that of cells not exposed to HGF (Figs. 6 B and S5 B). Thus, HGF-induced cell migration associates with the formation of prominent ventral stress fibers in a Src-FAK–dependent manner. The distribution of phosphorylated myosin light chain (pMLC) between those stress fibers and the cortex revealed an enrichment of pMLC at noncortical stress fibers upon HGF treatment (Fig. 6 A). In untreated MDCK colonies, pMLC density was about twice as high at the cortex as in ventral stress fibers (Fig. 6 C). Exposure to HGF reversed this distribution, as a result of a significant increase of pMLC density in stress fibers up to a value almost twice as high as at the cortex in the same condition (Fig. 6 C). In addition, exposure of HGF-treated cells to PP1 or PF228 abolished the pMLC distribution reversal induced by HGF (Figs. 6 C and S5 B). Altogether, these results show that migrating cells undergo a Src-FAK–dependent

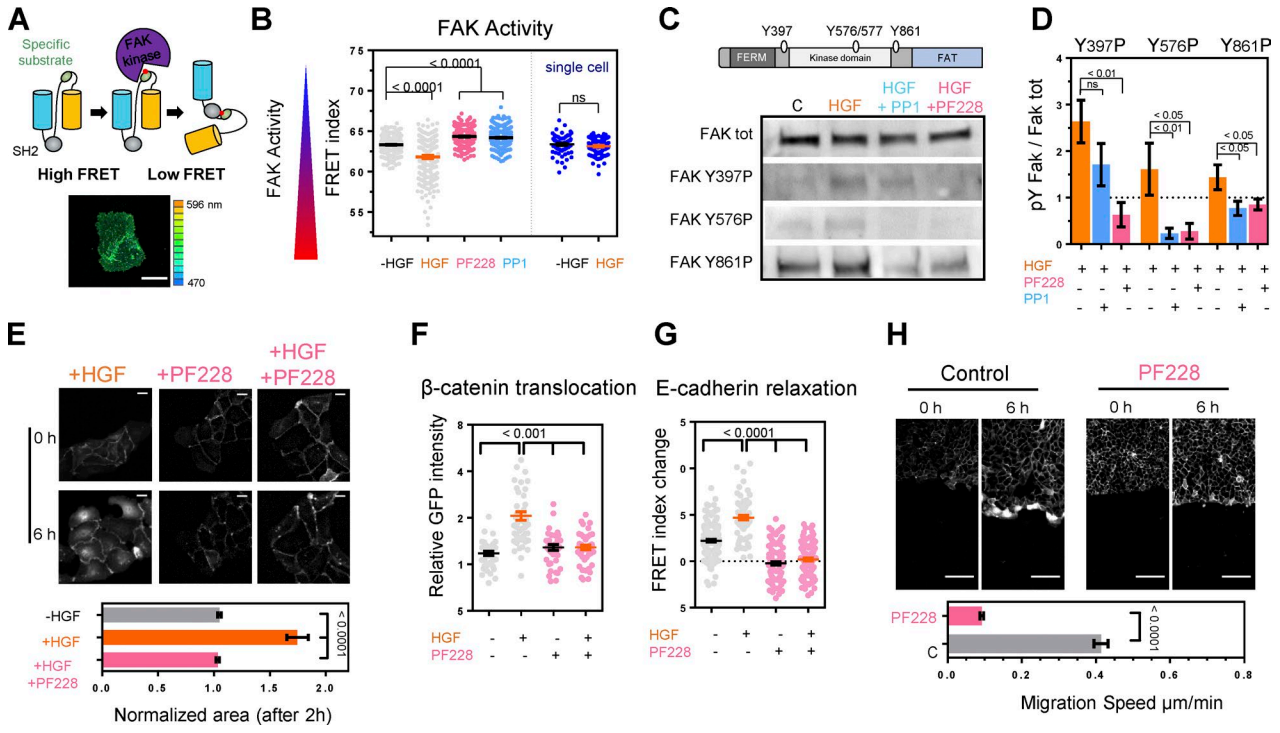

Figure 5. **FAK activity is required and activated by Src under stimulation. (A)** FAK kinase activity FRET biosensor. The higher the activity, the lower the FRET index. **(B)** FRET index (averaged over the whole cell) of the stably expressed FAK biosensor in unstimulated (n = 593), 4-h HGF-treated (n = 183), PF228-treated (n = 455), PP1-treated (n = 392) cells, single cells (n = 74), and 4-h HGF-treated single cells (n = 108), confluent cells (n = 91), and 4- to 5-h HGF-treated confluent cells (n = 202). ns, not significant. **(C)** Top: FAK domain organization and tyrosine sites. Bottom: Typical Western blot from lysates of unstimulated and HGF-treated (3 h) with or without PP1 or PF228. **(D)** Phosphorylation levels FAK Y397, Y576/577, Y861 normalized to total FAK level from Western blots of cells treated as in panel c (n = 7 lysates). **(E)** Top: Typical micrographs of GFP-β-catenin cells with and without HGF and PF228. Bottom: Area after 2 h normalized by the area at t = 0 for unstimulated cells, HGF-treated (data from Fig. S1 I), and HGF- and PF228-treated cells (n = 10 cells). **(F)** GFP intensity in the nucleus (relative to cytoplasm) of GFP-β-catenin 5 h with or without HGF (50 ng/ml; data from Fig. 1 E), and with PF228 (10 µM) with or without HGF (n = +/− 37/43 cells). **(G)** FRET index change of EcadTSMod in cells 5 h with and without HGF (50 ng/ml; data from Fig. 1 D), and with PF228 (25 µM) with or without HGF (n = +/− 110/99 cells). **(H)** Top: Typical micrographs of wounded sheet migration of GFP-β-catenin cells with and without (same control as in Fig. 3 D) PF228 (25 µM). Bottom: Migration speed (mean distance traveled by cell front per hour) with or without (same control as Fig. 3 D) PF228 (25 µM; n = 121 cells). Bars: (wound healing) 100 µm; (FAK sensor) 20 µm. Two-tailed Mann–Whitney or Kruskal–Wallis tests. Values plotted are mean ± SEM.

enrichment of ventral stress fibers that capture pMLC at the expense of the cortex.

To assess to what extent this cytoskeleton remodeling contributed to E-cadherin relaxation in migrating cells, we generated a molecular tension sensor of an E-cadherin-α-catenin chimera (E-α-TSMod) in which the β-catenin–binding site of E-cadherin was replaced by a truncated α-catenin lacking the β-catenin–binding domain (Fig. 6 D). By design, such a construct can relax only upon cytoskeleton relaxation or detachment from the actin-binding domain of α-catenin. Inhibition of actin polymerization led to a significant increase of FRET at cell–cell contacts in cells stably expressing E-α-TSMod compared with untreated cells (Fig. S5 C), consistent with a relaxation of cytoskeleton-induced tension. We tested next whether such a mere relaxation of cytoskeleton could suffice to relax E-α-TSMod tension in migration-induced cells. In wounded monolayers, E-α-TSMod exhibited a FRET higher in leader cells than in followers (Fig. 6 E), just as EcadTSMod did (Fig. 1 A). Consistently, E-α-TSMod exhibited a FRET higher in HGF-treated cells than in untreated cells (Fig. 6 F), just as EcadTSMod did (Fig. 1 D). Altogether, these results show that β-catenin release is dispensable for the tension relaxation of its E-cadherin in migration-induced cells, and are consistent with a tension relaxation only caused by cytoskeleton remodeling. Thus, Src-FAK–dependent actomyosin remodeling appears sufficient to explain E-cadherin relaxation.

Discussion

We used molecular tension microscopy (Gayrard and Borghi, 2016) to assess E-cadherin tension in epithelial cells induced to migrate upon exposure to HGF or after wound healing. Using instrument-specific FRET index to FRET efficiency calibration (Fig. S5 D; see Materials and methods) and previously published FRET efficiency to force calibration (Grashoff et al., 2010), we estimate that E-cadherin tension typically loses a couple piconewtons in cells induced to migrate (Fig. 1), a variation consistent with previous observations in this protein and others (Grashoff et al., 2010; Borghi et al., 2012). This tension decrease is spatially and temporally graded, and is reversible in collectively migrating cells (Fig. S1 B). The gradient of E-cadherin tension is reminiscent of that of intercellular tugging forces predicted from cell substrate traction stress previously reported in large epithelial colonies (Trepat et al., 2009). Thus, molecular and cell-scale force variations appear to correlate between E-cadherin and cell–cell contacts at the multicellular scale, just as they do between vinculin and focal adhesions at the cell scale

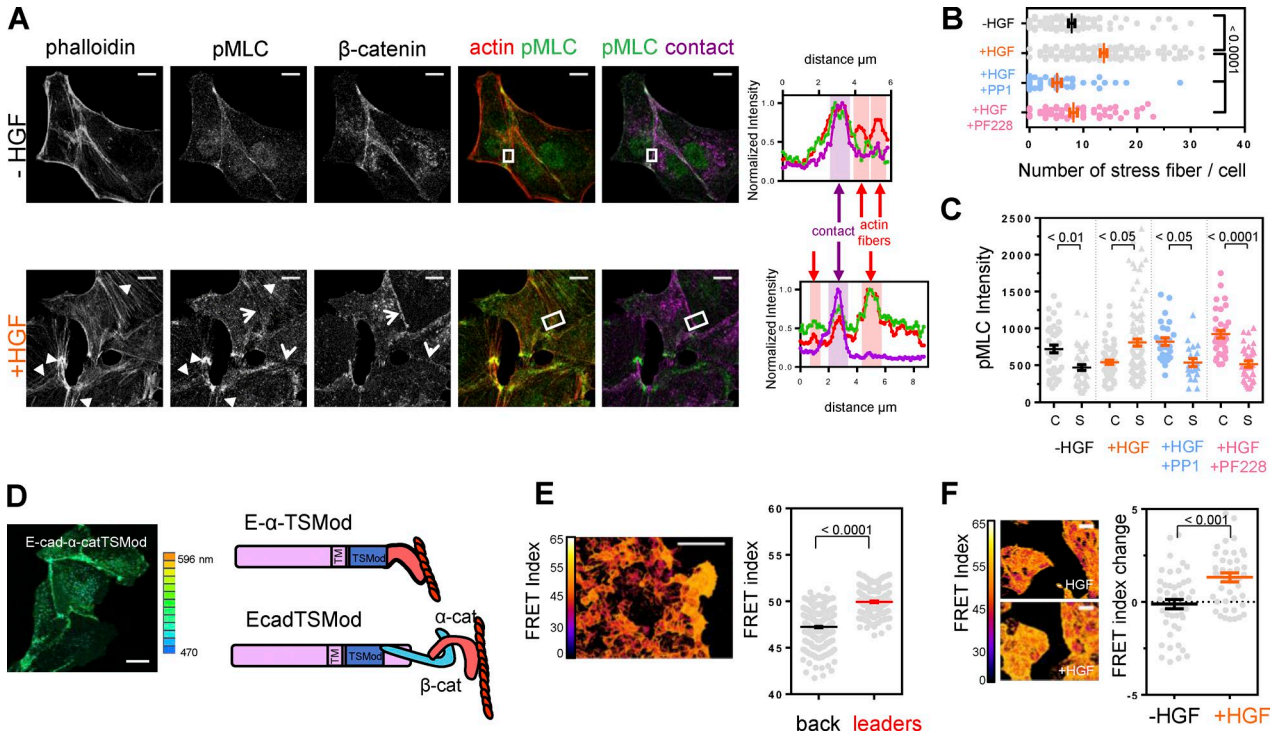

Figure 6. **Src-FAK–dependent actomyosin remodeling is sufficient for E-cadherin relaxation, and dissociation of β-catenin is not required. (A)** MDCK cells treated 4 h with or without HGF and stained with phalloidin, for pMLC and β-catenin. Arrowheads indicate fibers enriched in pMLC. Empty arrows indicate a cortex devoid of pMLC. Normalized intensity profiles of actin (phalloidin), pMLC, and contacts (β-catenin) of boxed regions shown on the right with same color code. **(B)** Stress fiber number per cell for conditions shown in panel a and Fig. S5 B (n = –HGF 99, +HGF 147, +HGF+PP1 68, +HGF+PF228 50 cells). **(C)** pMLC density at the cortex (C) or in stress fibers (S) for conditions shown in panel a and Fig. S5 B (n = C/S –HGF 40/45, +HGF 61/107, +HGF+PP1 26/20, and +HGF+PF228 35/33 cells). **(D)** Typical expression pattern and schematics of the β-catenin-less actin-binding E-α-TSMod chimera compared with EcadTSMod. **(E)** FRET index of E-α-TSMod in a wounded MDCK sheet. Top: Typical map. Bottom: FRET index of E-α-TSMod in leader (n = 135) and back (n = 245) cells of a wounded sheet. **(F)** FRET index of E-α-TSMod in cells with and without HGF (50 ng/ml). Top: Typical map. Bottom: FRET index change of E-α-TSMod 5 h after addition (n = 46 cells) or not (n = 45) of HGF (50 ng/ml). Bars, 20 µm. Two-tailed Mann–Whitney or Kruskal–Wallis tests. Values plotted are mean ± SEM.

(Sarangi et al., 2017). Intriguingly, however, E-cadherin tensions and cell–cell tugging forces do not appear to correlate in cell pairs (Sim et al., 2015), perhaps because such a correlation is an emergent property of large multicellular assemblies.

In addition, we showed that β-catenin nuclear accumulation and transcriptional activity associate with E-cadherin relaxation, in both HGF- and wound-induced migrating cells (Fig. 1), supporting it is a common feature of cells induced to migrate upon various stimulations. Moreover, we showed that β-catenin nuclear accumulation is selective and a consequence of a substantial release from the membrane, specifically in migrating cells (Fig. 2), consistently with the cytoplasmic accumulation of α-catenin (Fig. S1 H), because α-catenin must be released from the membrane if β-catenin is. Quantitative models have been devised to describe β-catenin cellular homeostasis and signaling kinetics (MacLean et al., 2015), initially focusing on β-catenin destruction complex and the influence of Wnt (Lee et al., 2003), to later include sequestration by E-cadherin (van Leeuwen et al., 2007), and shuttling between nucleus and cytoplasm (Schmitz et al., 2013). Assuming no specific underlying molecular mechanisms, we encapsulate these features in a model sufficient to test the contribution of membrane-bound β-catenin release to the nuclear pool. We show that no changes in β-catenin degradation and synthesis rates or membrane pool capacity explain β-catenin nuclear accumulation in migration-induced cells (Fig. S2). Indeed, although we observe that HGF stimulation slows down β-catenin degradation (Fig. S2 E), as previously seen in other model systems (Papkoff and Aikawa, 1998; Ishibe et al., 2006; Koraishy et al., 2014), degradation is too slow compared with exchange between pools, and is notably lower in confluent cells, which exhibit no nuclear β-catenin, than in leader cells, which exhibit nuclear β-catenin. Thus, noticeable variations of β-catenin degradation rate can occur and yet be insufficient for a regulation of nuclear β-catenin. More important changes are needed to regulate previously documented β-catenin signaling from the cytoplasm. Indeed, we confirm that pharmacological impairment of degradation leads to β-catenin nuclear accumulation (Fig. 2). However, we further show that such impairment does not result in membrane β-catenin release, nor does it affect E-cadherin tension (Fig. 2). Therefore, E-cadherin tension relaxation associates with β-catenin release from the membrane, rather than with β-catenin nuclear accumulation itself, and may not be attributed to downstream effects of β-catenin–dependent gene expression.

Finally, photoconversion experiments show that although membrane β-catenin translocates into the nucleus within minutes, it escapes the nucleus in the meantime (Fig. 2). Thus, to maintain high nuclear β-catenin levels for durations up to hours, as we observe upon HGF stimulation or wound healing, cells must constantly feed the nucleus, meanwhile replenishing their membrane reservoir. As for Wnt-induced β-catenin signaling, continuous β-catenin synthesis appears to also be required in migration-induced cells.

Src-induced phosphorylation of β-catenin was proposed to cause β-catenin dissociation from E-cadherin and subsequent

nuclear activity whether upon mechanical cues (Desprat et al., 2008; Whitehead et al., 2008; Brunet et al., 2013; Benham-Pyle et al., 2016), or stimulation by HGF (Monga et al., 2002). Here, we confirm Src activity requirement for β-catenin nuclear translocation and activity but also demonstrate it for E-cadherin relaxation (Fig. 4). This suggests that E-cadherin behaves as a mechanosensor of intracellular activity acting downstream of, rather than in combination with, Src. We also show that Src activity is permissive (Fig. S3 A), as in the gastrulating *Drosophila melanogaster* embryo (Desprat et al., 2008). In support for a role for β-catenin phosphorylation in this context, the affinity of the E-cadherin/β-catenin complex was shown to decrease upon β-catenin phosphorylation by Src in vitro, to a level similar to that of the phospho-impaired β-catenin tyrosine mutant Y654E (Roura et al., 1999), which also displays impaired affinity for E-cadherin in vivo (van Veelen et al., 2011). However, increased β-catenin phosphorylation does not appear to affect the complex stability in Src-transformed cells, whether MDCK or other lines (Hamaguchi et al., 1993; Reynolds et al., 1994; Papkoff, 1997), and β-catenin appeared dispensable for cadherin-based adhesion weakening upon overexpression of Src (Takeda et al., 1995). In addition, evidence for a substantial release of phosphorylated β-catenin from the membrane was unclear (Zeng et al., 2006; van Veelen et al., 2011; Brunet et al., 2013). Moreover, the same phospho-impaired mutant is able to rescue intercellular adhesion in a null background in culture and in vivo (Tominaga et al., 2008; van Veelen et al., 2011). Here, we show that phospho-impaired and phospho-mimic β-catenin mutants display an overall behavior similar to that of their WT counterpart upon HGF stimulation, all showing a membrane localization before nuclear translocation (Fig. 4), ruling out β-catenin as the most relevant direct Src target causing the complex disruption and effects attributed to it.

We further show that neither E-cadherin nor p120 are relevant direct Src targets. Indeed, the E-cadherin phospho-impaired mutant that favors p120 binding against endocytosis-inducing Hakai (Ishiyama et al., 2010) behaves just like WT E-cadherin in response to HGF or wound stimulation (Fig. 4). A previous study had proposed a role for endocytosis, either of E-cadherin or of other factors required for β-catenin transcription, in β-catenin signaling (Howard et al., 2011). Our results thus invalidate the requirement of Src-induced increase of E-cadherin endocytosis for E-cadherin relaxation and β-catenin translocation and are more consistent with a nuclear β-catenin originating from an E-cadherin pool at the plasma membrane.

Moreover, an E-cadherin chimera that can relax only through remodeling of the cytoskeleton to which it binds exhibits the same behavior as WT E-cadherin upon HGF or wound stimulation (Fig. 6). These results support a model by which E-cadherin relaxation and β-catenin release occur after cytoskeleton remodeling involving remote Src targets, rather than as a consequence of dissociation of the complex triggered by local Src-dependent phosphorylations. Consistently, a minimal E-cadherin/β-catenin/α-catenin complex dissociates faster from the actin cytoskeleton when mechanically relaxed in vitro (Buckley et al., 2014), by virtue of a catch-bond between, presumably, α-catenin and actin. In our experiments, simultaneous E-cadherin relaxation and β-catenin nuclear translocation from the membrane may just reflect a similar bond behavior between E-cadherin and β-catenin.

In cancer cells, exogenous expression of constitutively active Src impairs E-cadherin recruitment to cell–cell contacts in a FAK phosphorylation-dependent manner (Avizienyte et al., 2002). Here, we show in normal epithelial cells that the Src-FAK pathway is in fact involved in the regulation of E-cadherin and β-catenin at the membrane downstream of HGF and wounding (Fig. 5). More precisely, FAK activity is required downstream of permissive Src activity for E-cadherin relaxation and β-catenin nuclear translocation in migration-induced cells. Notably, FAK is activated upon HGF stimulation whereas Src is not, and the phosphorylation pattern of FAK upon HGF stimulation also shows partial, Src-independent autophosphorylation. The dependence of FAK autophosphorylation on Src and non-Src cues supports an integrative role of this kinase, which would thereby be able to sum signals of different types into a single graded output. This ability may also explain how Src Y527F bypasses HGF or wound stimulations without itself being downstream of these cues (Fig. S4).

As FAK activation is non–cell autonomous and requires multicellular deconfinement just as E-cadherin relaxation and β-catenin translocation do, we propose that the mere release of steric constraints from neighbor cells is the Src-independent cue that contributes to FAK activation. Consistently, under HGF stimulation, MDCK colonies can scatter and disrupt their cell–cell contacts only provided invadable room is available (Maruthamuthu and Gardel, 2014), and confluence prevents FAK interactions despite activation of HGF receptor cMET in other epithelial cell lines (Ishibe et al., 2006). Moreover, multicellular deconfinement is thought to underlie the similar effects on proliferation of wound healing and tissue stretching (Gudipaty et al., 2017), which, together with a variety of other mechanical cues such as substrate stiffness, has been involved upstream of FAK activation (Zebda et al., 2012). FAK's ability to self-activate by autophosphorylation, thus possibly autonomously from any other biochemical input, and computational evidence for a force-induced FAK activation (Zhou et al., 2015) support a direct role of mechanical tension on FAK in its activation. Finally, we show that FAK is required for cell spreading and concomitant cytoskeleton remodeling (Figs. 6 and S5). In turn, actomyosin remodeling involves a redistribution of phospho-myosin to ventral stress fibers at the expense of the cortex, where, consistently, cytoskeleton relaxation or detachment from the cadherin/catenin complex is sufficient to induce E-cadherin relaxation (Fig. 6).

Altogether, these results are consistent with a general role of cadherins as mechanosensors of intracellular mechanics, here the cortical/ventral contractility balance downstream of Src- and multicellular confinement–dependent FAK activation and cell spreading, and, selectively, upstream β-catenin signaling (Fig. 7). Independently of phosphorylations of the cadherin/catenin complex causing its dissociation or endocytosis from the membrane, membrane β-catenin is moreover sufficient to feed the nuclear pool, to which other β-catenin signaling regulatory mechanisms do not appear to contribute substantially.

Materials and methods

Cell lines

MDCK type II G cells were cultured at 37°C and 5% CO_2 in DMEM supplemented with 10% (vol/vol) FBS with low glucose (1 g/liter) and 200 mM G418 for stably expressing tagged proteins of interest (EcadTSMod, E-α-TSMod, EcadTSModΔCyto, E-cadherin-GFP, mMaple or GFP-β-catenin, Src Sensor, FAK sensor, TOPdGFP, FAK-GFP, and

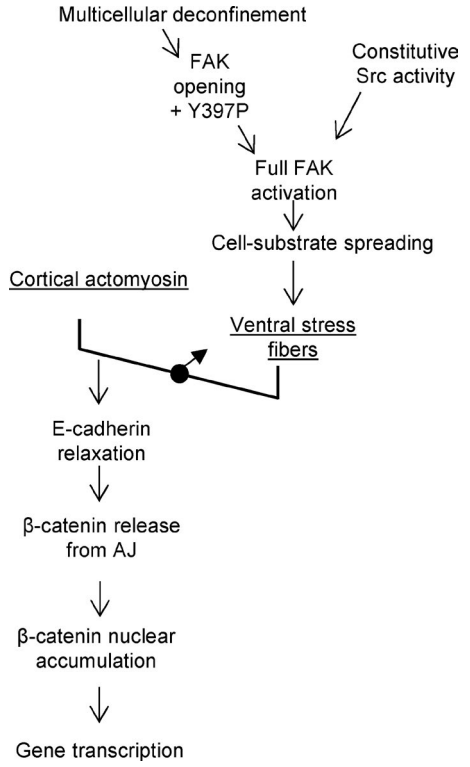

Figure 7. **Working model.** See text for details.

corresponding mutants). Cell lines expressing E-cadherin-GFP, α-catenin-GFP and GFP-β-catenin were a gift from W.J. Nelson (Stanford University, Stanford, CA), and TOPdGFP was a gift from C. Gottardi (Northwestern University, Chicago, IL). Before stimulation with HGF, cells were grown in DMEM supplemented with 0.5% FBS for 12 h.

Plasmids were transfected using Turbofect according to the instructions of the manufacturer (Thermo Fisher Scientific). Stable cell lines were obtained by FACS after 2 wks of selection at 400 nM G418. MDCKs expressing β-catenin constructs were selected from clones that stably expressed low levels, to avoid overexpression artifacts characterized by constitutive β-catenin accumulation in the cytoplasm and the nucleus (Fig. S1 G).

Plasmids

Mutants of GFP-β-catenin (Y654→E or F), EcadTSMod (Y754-Y755-Y756→FFF), E-cadherin-GFP (Y754-Y755-Y756→FFF or EEE), and mCherry-c-Src (Y527→F) were made with the Quikchange II XL site-directed mutagenesis kit (Agilent) on pEGFP-C1 β-catenin (from E. Schuman, Max Plank Institute for Brain Research, Frankfurt, Germany; 16071; Addgene), EcadTSMod, and mCherry c-Src (from M. Davidson, Florida State University, Tallahassee, FL; 55002; Addgene) with the following respective primers: 5′-CCAGGAATGAGG GTGTTGCAACAGAAGCAGCTGCAGTGC-3′, 5′-CTGCAGCTG CAAATGTTGCAACACCCTCATTCC-3′, 5′-GATGACACCCGG GACAATGTTTTTTTCTTTGATGAAGAAGGAGGTGG-3′, 5′-GAT GACACCCGGGACAATGTTTTTTTCTTTGATGAAGAAGGAGGT GG-3′, 5′-GATGACACCCGGGACAATGTTGAAGAGGAAGAT GAAGAAGGAGGTGG-3′, and 5′-CAGAGCCCCAGTTCCAGC CTGGAGAG-3′ and the corresponding reverse primers.

Lyn-FAK and Kras-Src biosensors were adapted from biosensors (78302 and 78299; Addgene) shared by Y. Wang (University of California, San Diego, San Diego, CA) using In-fusion HD cloning kit (TaKaRa Bio): Lyn-FAK PCR forward 5′-GCCCGCATGCATTGGTATTTT GGG-3′, reverse 5′-GGTCTTCATGTCCACGCCGT-3′; Kras-Src PCR forward 5′-GCCCGCATGCATTGGTATTTTGGG-3′, reverse 5′-GGG ATCCTTATCGTCATCGTCGT-3′. CFP was replaced by mTFP1 from the EcadTSMod construct: PCR forward 5′-ACGGCGTGGACATGA AGACCATGGTCTCGAAAGGCGAAGAAACAAC-3′, reverse 5′-ATACCAATGCATGCGGGCCTTGTAAAGTTCATCCATTCCAT-3′ for Lyn-FAK; PCR forward 5′-CGACGATGACGATAAGGATCC CATGGTCTCGAAAGGCGAAGAAACAAC-3′, reverse 5′-ATA CCAATGCATGCGGGCCTTGTAAAGTTCATCCATTCCAT-3′ for Kras-Src. pEGFP-FAK was a gift from J.-L. Guan (University of Cincinnati, Cincinnati, OH).

E-α-TSMod was generated from EcadTSMod aa 1–810 (PCR forward 5′-TTTTAAAGCGGCCGCGACTCTAGATCAT-3′, reverse 5′-TTTGTTTCCAATTTCATCAGGATTGGCAGG-3′) and α-E-catenin 270–906 (PCR forward 5′-CCTGATGAAATTGGAAACGGT ACCCAGGGTGGCAGTGGCGGAGAGCTGGCATA-3′, reverse 5′-GTCGCGGCCGCTTTAGTCGACGATGCTGTCCATGGCTTTGAA CTCGCTCAGG-3′) from pEGFP-α-E-catenin (shared by W.J. Nelson) using In-fusion HD Cloning kit.

mMaple-β-catenin was generated from mMaple cDNA (shared by M. Nolmann, Centre National de la Recherche Scientifique, Université Montpellier, Montpellier, France) into the pEGFP vector (PCR forward 5′-CAGCAGTCATATCTGGACTCT-3′, reverse 5′-AAACAT AATGAGGACCTACAC-3′). Constructs were verified by digestion, gel electrophoresis, and sequencing of coding regions.

Chemical inhibitors and biochemical perturbations

HGF was used at 50 ng/ml final concentration on starved cells (H5691; 20 µg/ml in PBS stock; Sigma-Aldrich). Cytochalasin B was used at 10 µM final concentration (10 mg/ml in DMSO stock; C6762; Sigma-Aldrich). Specific Src family inhibitor PP1 (10 mM in DMSO stock; 567809; Merck Chemicals) or specific FAK inhibitor PF228 (10 mM in DMSO stock; PZ0117; Sigma-Aldrich) were used at a final concentration of 25, 75, and 10 µM, respectively. LiCl solution was used at 30 mM final concentration (105679; Merck Chemicals).

HGF stimulation and scratch assay

Cells were plated on glass coverslips coated with 50 µg/ml human type IV collagen (C7521; Sigma-Aldrich) 24 h before imaging, at 15% density (~200,000 cells) for HGF stimulation of subconfluent colonies, or at confluence (~2 million cells) for wound healing assays and HGF experiments on confluent monolayers. Cells were exposed to HGF 12 h after starvation and imaged at $t = 0$, and then every 20 min for 4–7 h (usually 5 h) after HGF addition. Wound healing assays were performed either scratching the monolayer with a 200-µl pipette tip and washing detached cells or removing a two-well silicone insert (Ibidi). For isolated cell experiments, cells were plated 8 h before imaging and starved for 2–3 h before adding HGF, to minimize cell doublets caused by cell division. Live cells were imaged in FluoroBrite DMEM medium (Life Technologies) without phenol red supplemented with 10% or 0.5% FBS depending on experiments, 1 U/ml penicillin, 20 mM Hepes, and 2.5 mM L-glutamine, at 37°C, and 5% CO_2.

Western blot

Cells were washed, lysed with ice-cold RIPA buffer supplemented with Protease Inhibitor Mini Tablets (Thermo Fisher Scientific) and PhosphoSTOP (Phosphatase Inhibitor Cocktail Tablets; Roche). Extracts were centrifuged at 11,000 *g* for 15 min at 4°C, and supernatants were collected and analyzed by electrophoresis under reducing conditions using NuPAGE 4–12% Bis-Tris gels (Invitrogen). Proteins were transferred to nitrocellulose (Whatman), blocked, and probed with primary antibodies against FAK, p-FAK Y397, p-FAK Y576/577, p-FAK Y86

(610088; BD Sciences; 11765; Santa Cruz Biotechnologies; 3281P; Cell Signaling Technology; and 44626; Invitrogen, respectively) or primary antibodies against E-cadherin, β-catenin, or α-tubulin (clone 36-610181; BD Sciences; CM1181; ECM Biosciences; and T9026; Sigma-Aldrich). Primary antibodies were detected with anti-mouse or anti-rabbit HRP-conjugated secondary antibodies (Life Technologies) and visualized by enhanced chemiluminescence with SuperSignal West Femto or Pico kits (Thermo Fisher Scientific). Primary and secondary antibodies were prepared in blocking buffer plus 0.1% Tween-20.

Immunostaining

Cells were washed, fixed in 4% PFA (Electron Microscopy Science) for 10 min at 4°C, rinsed with PBS, permeabilized with a solution of 0.5% Triton X-100 in PBS for 5 min, incubated for 5 min with 5mM NH_4Cl, and blocked in PBS containing 1% BSA (Jackson Immunology) and 1% goat/donkey serum (Sigma-Aldrich) for 30 min at RT. Cells were stained with phalloidin-Alexa Fluor 550 (Molecular Probes), mouse anti–β-catenin (CM1181; ECM Biosciences), rabbit anti–myosin light chain phospho S20 pMLC (ab2480; Abcam) primary antibodies (1 h in blocking buffer at RT), followed by incubation with the appropriate Dylight 480 or 650 secondary antibody (Thermo Fisher Scientific) for 45 min at RT. Coverslips were mounted in Fluoromount medium (Sigma-Aldrich), and fluorescent images were acquired on confocal microscopes (LSM 780 or 710; Zeiss) with a 63×/1.4NA oil-immersion objective.

Image acquisition

Fluorescence live-cell imaging. Cells were viewed with a 20×/0.4NA dry objective (HCX PL Fluotar) on a wide-field DMI6000 microscope (Leica) to assess β-catenin-GFP localization and cell migration in HGF and wound healing experiments.

FRET imaging. Spectral imaging was performed on confocal microscopes (LSM 780 or 710; Zen software) with a 63×/1.4NA oil-immersion objective. mTFP1 was excited by the 458-nm line of a 30-mW argon laser. Emission was sampled at a spectral resolution of 9.8 nm for LSM 710 and 8.7 nm for LSM 780 within the 470- to 600-nm range, every 20 min for ∼15 h at ∼10 different positions. Molecular tension sensors were imaged on the LSM 710, and kinase biosensors were imaged on the LSM 780.

Photoconversion. Photoconversion of β-catenin mMaple was achieved with the 405-nm laser beam at 20% power with 20 repetitions at ∼3.15 µs/pixel at a selected region on LSM 710 or 780 microscope. Images from green channel (488-nm excitation) and red channel (561-nm excitation) were acquired every 1 min for local photoconversion in a contact zone and every 20 min for entire cell photoconversion in degradation/synthesis experiments. Transmission images were used to monitor cell contour outlines and nucleus.

FRAP. FRAP experiments were performed on a DMI6000 microscope equipped with a CSU-X1 spinning-disk head (Yokogawa), a 63×/NA 1.2 oil-immersion objective, and an EMCCD camera (Photometrics QuantEM). A FRAP Head (Roper scientific) equipped with a 473-nm diode laser (100 mW) was used to perform bleaching (100% laser power), and image acquisitions were performed with a 491-nm diode laser (50 mW) at 30% laser power every 1 s for 5 s prebleach, then every 1 s for 30 s, 10 s for 120 s, and 30 s for 400 s after bleach.

FRET analysis

Fluorescent images were analyzed in ImageJ using the Fiji distribution and the publicly available PixFRET plugin. All channels were background-subtracted, Gaussian smoothed (radius = 1 pixel), and thresholded (above the first ∼3–5% of the 12-bit range). The FRET index was computed as $I_{EYFP}/(I_{mTFP} + I_{EYFP})$. For quantification, the FRET index was then averaged over the segmented cell–cell contacts in all experiments with HGF. In all figures with EcadTSMod and its control variants, only the signal from intercellular contacts, as shown in Fig. S1 A, was considered in the analysis. In all figures where the "leaders" condition was considered, FRET was analyzed from the lamellipodium, and where the "back" condition was considered, FRET was analyzed from intercellular contacts of follower cells hundreds of micrometers away from the border of the wound. For single-cell experiments, FRET was analyzed from the basal membrane signal because of the absence of intercellular contacts. For Src and FAK FRET sensors, the signal from the whole cell was considered for analysis, with no excluded region. FRET index to FRET efficiency calibration was performed with mTFP-TRAF-Venus and mTFP-5aa-Venus constructs obtained from R.N. Day (Indiana University, Bloomington, IN). The measured FRET index values were paired to previously published FRET efficiency values for those constructs (Fig. S5 D). Linear interpolation between those values was used to infer FRET efficiencies from all other FRET index measurements in our experiments.

Fluorescence, FRAP, and photoconversion analysis

Fluorescent images were analyzed in ImageJ using the Fiji distribution. All channels were background-subtracted. Mean pixel intensity was measured within the boundaries of regions of interest (ROIs; contacts, cytoplasm, and nucleus), which were determined based on transmission or fluorescence images.

For FRAP and photoconversion, data were normalized and fitted with the single exponential recovery model $F = F_0 + F_\tau\,(1 - \exp(-t/\tau))$, where F_0 is the fluorescence that recovers before the first time point, and F_τ is the fluorescence of the mobile fraction characterized by the turnover time τ. Half-times and half-lives are $\tau_{1/2} = \tau.\ln 2$.

Quantification of immunostaining: analysis of the number of actin fibers and pMLC density

In ImageJ, raw images were background-subtracted and thresholded (above the first 5% of the 12-bit range), and stress fibers were manually counted. To quantify changes in pMLC density, cortex and stress fiber ROIs were segmented based on the membrane β-catenin and phalloidin stainings: membrane β-catenin defined the cortex, and phalloidin staining not overlapping membrane β-catenin and excluding colony edges defined stress fibers. pMLC density was the mean pixel intensity of pMLC staining in these ROIs.

Statistical analysis

Data are presented as mean ± SEM. P-values were calculated in GraphPad Prism V software from unpaired, nonparametric, two-tailed tests (Mann–Whitney for two conditions or Kruskal–Wallis for more) when comparing distributions, and from extra sum-of-squares F tests when comparing fit parameters.

Kinetic three-compartment model

We consider β-catenin concentrations C, M, and N in the cytoplasm, at the membrane, and in the nucleus, respectively. If the membrane pool is not saturated, balance equations are

$$\frac{dC}{dt} = s - k_{cd}C - k_{cm}C + k_{mc}M - k_{cn}C + k_{nc}N,$$

$$\frac{dN}{dt} = -k_{nd}N + k_{cn}C - k_{nc}N,$$

and

$$\frac{dM}{dt} = -k_{md}M + k_{cm}C - k_{mc}M,$$

with a protein synthesis rate s, degradation rates k_{xd}, and apparent exchange ratesk_{xy}, where x,y = m at the membrane, n in the nucleus, and c in the cytoplasm.

Steady-state solutions are as follow:

$$N = \frac{k_{cn}\, s\,(k_{mc}+k_{md})}{k_{mc}k_{cd}k_{nd}+k_{cd}k_{md}k_{nd}+k_{mc}k_{nd}k_{cn}+k_{md}k_{cd}k_{cn}+, \\ k_{md}k_{nd}k_{cm}+k_{mc}k_{cd}k_{nc}+k_{cd}k_{md}k_{nc}+k_{md}k_{cm}k_{nc}},$$

$$C = \frac{s\,(k_{mc}+k_{md})(k_{nd}+k_{nc})}{k_{mc}k_{cd}k_{nd}+k_{cd}k_{md}k_{nd}+k_{mc}k_{nd}k_{cn}+k_{md}k_{cd}k_{cn}+, \\ k_{md}k_{nd}k_{cm}+k_{mc}k_{cd}k_{nc}+k_{cd}k_{md}k_{nc}+k_{md}k_{cm}k_{nc}},$$

and

$$M = \frac{k_{cm}\, s\,(k_{nc}+k_{nd})}{k_{mc}k_{cd}k_{nd}+k_{cd}k_{md}k_{nd}+k_{mc}k_{nd}k_{cn}+k_{md}k_{cd}k_{cn}+. \\ k_{md}k_{nd}k_{cm}+k_{mc}k_{cd}k_{nc}+k_{cd}k_{md}k_{nc}+k_{md}k_{cm}k_{nc}}$$

The β-catenin *N/M* then is

$$\frac{N}{M} = \frac{k_{cn}(k_{mc}+k_{md})}{k_{cm}(k_{nc}+k_{nd})}.$$

In the low degradation rate limit (k_{md},$k_{nd} = k_{mc}$,k_{nc}), it is

$$\frac{N}{M} = \frac{K_{a,n}}{K_{a,m}},$$

where

$$K_{a,m} = \frac{k_{cm}}{k_{mc}}$$

and

$$K_{a,n} = \frac{k_{cn}}{k_{nc}}.$$

If the membrane pool is saturated, balance equations are

$$M = M_{max},$$

$$\frac{dC}{dt} = s - k_{cd}C - k_{cn}C + k_{nc}N,$$

and

$$\frac{dN}{dt} = -k_{nd}N + k_{cn}C - k_{nc}N.$$

Steady-state solutions are

$$M = M_{max},$$

$$N = \frac{k_{cn}\, s}{k_{cd}k_{nd}+k_{nd}k_{cn}+k_{cd}k_{nc}},$$

and

$$C = \frac{s(\,k_{nc}+k_{nd})}{k_{cd}k_{nd}+k_{nd}k_{cn}+k_{cd}k_{nc}}.$$

The β-catenin *N/M* then is

$$\frac{N}{M} = \frac{k_{cn}\, s}{M_{max}(k_{cd}k_{nd}+k_{nd}k_{cn}+k_{cd}k_{nc})}.$$

In the low degradation limit, it is

$$\frac{N}{M} = \frac{K_{a,n}}{M_{max}}K_p,$$

with

$$K_p = \frac{s}{k_{cd}}.$$

Although these solutions are sufficient to show the most substantial sources of nuclear β-catenin in our experiments (see Results section), it is also possible to further show binding/unbinding and endo/exocytosis of the β-catenin/E-cadherin complex. The model (Fig. S5 E) then is rewritten as:

$$\frac{dN}{dt} = k_{cn}B - k_{nc}N,$$

$$\frac{dB}{dt} = s - k_{cd}B - 2k_{+}B + k_{-}(M+C) - k_{cn}B + k_{nc}N,$$

$$\frac{dC}{dt} = k_{+}B - k_{-}C + k_{endo}M - k_{exo}C$$

and

$$\frac{dM}{dt} = k_{+}B - k_{-}M - k_{endo}M + k_{exo}C,$$

with B, M, and C as the concentrations of free cytoplasmic β-catenin, β-catenin/E-cadherin complex at the membrane, and in the cytoplasm. k_+ and k_- are the binding/unbinding rates, and k_{exo} and k_{endo} are the exo/endocytosis rates.

Steady-state solutions are

$$N = \frac{s\,k_{cn}}{k_{cd}\,k_{nc}} = K_p K_{a,n},$$

$$B = \frac{s}{k_{cd}} = K_p,$$

$$C = K_p K_{a,Ecad}\left(\frac{k_- + 2k_{endo}}{k_- + k_{endo} + k_{exo}}\right),$$

$$M = K_p K_{a,Ecad}\left(\frac{k_- + 2k_{exo}}{k_- + k_{endo} + k_{exo}}\right),$$

with

$$K_{a,Ecad} = \frac{k_+}{k_-}.$$

The β-catenin *N/M*s then are

$$\frac{N}{M} = \frac{K_{a,n}}{K_{a,Ecad}}\left(\frac{k_- + k_{exo} + k_{endo}}{k_- + 2k_{exo}}\right),$$

$$\text{if } k_{exo}, k_{endo} \gg k_-, \text{ then } \frac{N}{M} = \frac{K_{a,n}}{K_{a,Ecad}} \cdot \frac{1}{2} \cdot (1 + K_{exo/endo}),$$

with

$$K_{exo/endo} = \frac{k_{exo}}{k_{endo}},$$

$$\text{else, } \frac{N}{M} = \frac{K_{a,n}}{K_{a,Ecad}}.$$

These solutions explicitly display the dependence of *N/M* on E-cadherin binding whether in the fast unbinding limit ($k_- \gg k_{exo}$, and k_{endo}) or not. Nevertheless, the apparent exchange rates k_{CM} and k_{MC} measured by fluorescence recovery report the binding and unbinding rates k_+ and k_- only in the fast unbinding limit. Otherwise, they are influenced by

endo/exocytosis. Experimentally, we find that k_{CM}/k_{MC} do not appear to decrease upon migration induction (Fig. S2), as a decreased affinity in the fast unbinding limit would predict. Thus, our results rather support that faster endocytosis masks slower unbinding kinetics.

Online supplemental material

Fig. S1 contains images and data of wound healing assays, HGF stimulations, and Western blots of whole-cell lysates on cells expressing EcadTSMod, EcadTSModΔcyto, β-catenin-GFP, and α-catenin-GFP. Fig. S2 contains images, data, and model of β-catenin and E-cadherin turnover and exchange during wound healing and HGF stimulation. Fig. S3 contains images and data of Src sensor response to HGF, inhibitors and Src Y527F mutant, and EcadTSMod phosphomutant turnover and response to HGF and wound healing. Fig. S4 contains images and data of Src Y527F mutant localization and effects on E-cadherin and β-catenin. Fig. S5 contains images and data of HGF and inhibitor effects on the actomyosin cytoskeleton, FAK and the E-α-TSMod chimera, FRET efficiency/index calibration, and the augmented kinetic model.

Acknowledgments

We thank the members of the laboratory, E. Farge, R-M. Mège, and M. Thery, for insightful discussions; C. Garoche for preliminary experiments; and C.P. Toret for critical reading of the manuscript. We thank W.J. Nelson, C. Gottardi, E. Schuman, M. Davidson, Y. Wang, J-L. Guan, and M. Nolmann for sharing reagents.

This work is supported by the Centre National de la Recherche Scientifique, the Fondation ARC pour la Recherche sur le Cancer grant SFI20121205916), the Agence Nationale de la Recherche (grant ANR-13-JSV5-0007-01), a Fondation pour la Recherche Médicale fellowship (FDT20160435448 to C. Gayrard), and a L'Oréal-UNESCO "For Women in Science" 2016 fellowship (to C. Gayrard). We acknowledge the ImagoSeine core facility of the Institut Jacques Monod, member of IBiSA, and France-BioImaging (ANR-10-INBS-04) infrastructures.

The authors declare no competing financial interests.

Author contributions: C. Gayrard and N. Borghi designed the experiments; C. Gayrard, C. Bernaudin, C. Seiler, and N. Borghi contributed reagents; C. Gayrard, C. Bernaudin, and T. Déjardin performed the experiments; and C. Gayrard and N. Borghi analyzed the data and wrote the manuscript.

Submitted: 2 June 2017
Revised: 20 September 2017
Accepted: 4 December 2017

References

Avizienyte, E., A.W. Wyke, R.J. Jones, G.W. McLean, M.A. Westhoff, V.G. Brunton, and M.C. Frame. 2002. Src-induced de-regulation of E-cadherin in colon cancer cells requires integrin signalling. *Nat. Cell Biol.* 4:632–638.

Behrens, J., L. Vakaet, R. Friis, E. Winterhager, F. Van Roy, M.M. Mareel, and W. Birchmeier. 1993. Loss of epithelial differentiation and gain of invasiveness correlates with tyrosine phosphorylation of the E-cadherin/β-catenin complex in cells transformed with a temperature-sensitive v-SRC gene. *J. Cell Biol.* 120:757–766. https://doi.org/10.1083/jcb.120.3.757

Benham-Pyle, B.W., B.L. Pruitt, and W.J. Nelson. 2015. Mechanical strain induces E-cadherin-dependent Yap1 and -catenin activation to drive cell cycle entry. *Science.* 348:1024–1027. https://doi.org/10.1126/science.aaa4559

Benham-Pyle, B.W., J.Y. Sim, K.C. Hart, B.L. Pruitt, and W.J. Nelson. 2016. Increasing β-catenin/Wnt3A activity levels drive mechanical strain-induced cell cycle progression through mitosis. *eLife.* 5:e19799. https://doi.org/10.7554/eLife.19799

Borghi, N., and W.J. Nelson. 2009. Intercellular adhesion in morphogenesis: Molecular and biophysical considerations. *Curr. Top. Dev. Biol.* 89:1–32. https://doi.org/10.1016/S0070-2153(09)89001-7

Borghi, N., M. Sorokina, O.G. Shcherbakova, W.I. Weis, B.L. Pruitt, W.J. Nelson, and A.R. Dunn. 2012. E-cadherin is under constitutive actomyosin-generated tension that is increased at cell-cell contacts upon externally applied stretch. *Proc. Natl. Acad. Sci. USA.* 109:12568–12573. https://doi.org/10.1073/pnas.1204390109

Brunet, T., A. Bouclet, P. Ahmadi, D. Mitrossilis, B. Driquez, A.C. Brunet, L. Henry, F. Serman, G. Béalle, C. Ménager, et al. 2013. Evolutionary conservation of early mesoderm specification by mechanotransduction in Bilateria. *Nat. Commun.* 4:2821. https://doi.org/10.1038/ncomms3821

Buckley, C.D., J. Tan, K.L. Anderson, D. Hanein, N. Volkmann, W.I. Weis, W.J. Nelson, and A.R. Dunn. 2014. Cell adhesion. The minimal cadherin-catenin complex binds to actin filaments under force. *Science.* 346:1254211. https://doi.org/10.1126/science.1254211

Calalb, M.B., T.R. Polte, and S.K. Hanks. 1995. Tyrosine phosphorylation of focal adhesion kinase at sites in the catalytic domain regulates kinase activity: A role for Src family kinases. *Mol. Cell. Biol.* 15:954–963. https://doi.org/10.1128/MCB.15.2.954

Catimel, B., M. Layton, N. Church, J. Ross, M. Condron, M. Faux, R.J. Simpson, A.W. Burgess, and E.C. Nice. 2006. In situ phosphorylation of immobilized receptors on biosensor surfaces: Application to E-cadherin/β-catenin interactions. *Anal. Biochem.* 357:277–288. https://doi.org/10.1016/j.ab.2006.07.034

Clevers, H., and R. Nusse. 2012. Wnt/β-catenin signaling and disease. *Cell.* 149:1192–1205. https://doi.org/10.1016/j.cell.2012.05.012

de Rooij, J., A. Kerstens, G. Danuser, M.A. Schwartz, and C.M. Waterman-Storer. 2005. Integrin-dependent actomyosin contraction regulates epithelial cell scattering. *J. Cell Biol.* 171:153–164. https://doi.org/10.1083/jcb.200506152

Desprat, N., W. Supatto, P.A. Pouille, E. Beaurepaire, and E. Farge. 2008. Tissue deformation modulates twist expression to determine anterior midgut differentiation in Drosophila embryos. *Dev. Cell.* 15:470–477. https://doi.org/10.1016/j.devcel.2008.07.009

Dorsky, R.I., L.C. Sheldahl, and R.T. Moon. 2002. A transgenic Lef1/beta-catenin-dependent reporter is expressed in spatially restricted domains throughout zebrafish development. *Dev. Biol.* 241:229–237. https://doi.org/10.1006/dbio.2001.0515

Farge, E. 2003. Mechanical induction of Twist in the Drosophila foregut/stomodeal primordium. *Curr. Biol.* 13:1365–1377. https://doi.org/10.1016/S0960-9822(03)00576-1

Fernández-Sánchez, M.E., S. Barbier, J. Whitehead, G. Béalle, A. Michel, H. Latorre-Ossa, C. Rey, L. Fouassier, A. Claperon, L. Brullé, et al. 2015. Mechanical induction of the tumorigenic β-catenin pathway by tumour growth pressure. *Nature.* 523:92–95. https://doi.org/10.1038/nature14329

Fujita, Y., G. Krause, M. Scheffner, D. Zechner, H.E. Leddy, J. Behrens, T. Sommer, and W. Birchmeier. 2002. Hakai, a c-Cbl-like protein, ubiquitinates and induces endocytosis of the E-cadherin complex. *Nat. Cell Biol.* 4:222–231. https://doi.org/10.1038/ncb758

Gayrard, C., and N. Borghi. 2016. FRET-based molecular tension microscopy. *Methods.* 94:33–42. https://doi.org/10.1016/j.ymeth.2015.07.010

Grashoff, C., B.D. Hoffman, M.D. Brenner, R. Zhou, M. Parsons, M.T. Yang, M.A. McLean, S.G. Sligar, C.S. Chen, T. Ha, and M.A. Schwartz. 2010. Measuring mechanical tension across vinculin reveals regulation of focal adhesion dynamics. *Nature.* 466:263–266. https://doi.org/10.1038/nature09198

Gudipaty, S.A., J. Lindblom, P.D. Loftus, M.J. Redd, K. Edes, C.F. Davey, V. Krishnegowda, and J. Rosenblatt. 2017. Mechanical stretch triggers rapid epithelial cell division through Piezo1. *Nature.* 543:118–121. https://doi.org/10.1038/nature21407

Hamaguchi, M., N. Matsuyoshi, Y. Ohnishi, B. Gotoh, M. Takeichi, and Y. Nagai. 1993. p60v-src causes tyrosine phosphorylation and inactivation of the N-cadherin-catenin cell adhesion system. *EMBO J.* 12:307–314.

Hens, J.R., K.M. Wilson, P. Dann, X. Chen, M.C. Horowitz, and J.J. Wysolmerski. 2005. TOPGAL mice show that the canonical Wnt signaling pathway is active during bone development and growth and is activated by mechanical loading in vitro. *J. Bone Miner. Res.* 20:1103–1113. https://doi.org/10.1359/JBMR.050210

Howard, S., T. Deroo, Y. Fujita, and N. Itasaki. 2011. A positive role of cadherin in Wnt/β-catenin signalling during epithelial-mesenchymal transition. *PLoS One.* 6:e23899. https://doi.org/10.1371/journal.pone.0023899

Ishibe, S., J.E. Haydu, A. Togawa, A. Marlier, and L.G. Cantley. 2006. Cell confluence regulates hepatocyte growth factor-stimulated cell morphogenesis in a beta-catenin-dependent manner. *Mol. Cell. Biol.* 26:9232–9243. https://doi.org/10.1128/MCB.01312-06

Ishiyama, N., S.H. Lee, S. Liu, G.Y. Li, M.J. Smith, L.F. Reichardt, and M. Ikura. 2010. Dynamic and static interactions between p120 catenin and E-cadherin regulate the stability of cell-cell adhesion. *Cell.* 141:117–128. https://doi.org/10.1016/j.cell.2010.01.017

Koraishy, F.M., C. Silva, S. Mason, D. Wu, and L.G. Cantley. 2014. Hepatocyte growth factor (Hgf) stimulates low density lipoprotein receptor-related protein (Lrp) 5/6 phosphorylation and promotes canonical Wnt signaling. *J. Biol. Chem.* 289:14341–14350. https://doi.org/10.1074/jbc.M114.563213

Krieghoff, E., J. Behrens, and B. Mayr. 2006. Nucleo-cytoplasmic distribution of beta-catenin is regulated by retention. *J. Cell Sci.* 119:1453–1463. https://doi.org/10.1242/jcs.02864

Lee, E., A. Salic, R. Krüger, R. Heinrich, and M.W. Kirschner. 2003. The roles of APC and Axin derived from experimental and theoretical analysis of the Wnt pathway. *PLoS Biol.* 1:E10. https://doi.org/10.1371/journal.pbio.0000010

Lietha, D., X. Cai, D.F. Ceccarelli, Y. Li, M.D. Schaller, and M.J. Eck. 2007. Structural basis for the autoinhibition of focal adhesion kinase. *Cell.* 129:1177–1187. https://doi.org/10.1016/j.cell.2007.05.041

Loerke, D., Q. le Duc, I. Blonk, A. Kerstens, E. Spanjaard, M. Machacek, G. Danuser, and J. de Rooij. 2012. Quantitative imaging of epithelial cell scattering identifies specific inhibitors of cell motility and cell-cell dissociation. *Sci. Signal.* 5:rs5. https://doi.org/10.1126/scisignal.2002677

MacLean, A.L., Z. Rosen, H.M. Byrne, and H.A. Harrington. 2015. Parameter-free methods distinguish Wnt pathway models and guide design of experiments. *Proc. Natl. Acad. Sci. USA.* 112:2652–2657. https://doi.org/10.1073/pnas.1416655112

Maher, M.T., A.S. Flozak, A.M. Stocker, A. Chenn, and C.J. Gottardi. 2009. Activity of the β-catenin phosphodestruction complex at cell-cell contacts is enhanced by cadherin-based adhesion. *J. Cell Biol.* 186:219–228. https://doi.org/10.1083/jcb.200811108

Maruthamuthu, V., and M.L. Gardel. 2014. Protrusive activity guides changes in cell-cell tension during epithelial cell scattering. *Biophys. J.* 107:555–563. https://doi.org/10.1016/j.bpj.2014.06.028

Matsubayashi, Y., M. Ebisuya, S. Honjoh, and E. Nishida. 2004. ERK activation propagates in epithelial cell sheets and regulates their migration during wound healing. *Curr. Biol.* 14:731–735. https://doi.org/10.1016/j.cub.2004.03.060

Monga, S.P.S., W.M. Mars, P. Pediaditakis, A. Bell, K. Mulé, W.C. Bowen, X. Wang, R. Zarnegar, and G.K. Michalopoulos. 2002. Hepatocyte growth factor induces Wnt-independent nuclear translocation of beta-catenin after Met-beta-catenin dissociation in hepatocytes. *Cancer Res.* 62:2064–2071.

Mukherjee, M., S.Y. Chow, P. Yusoff, J. Seetharaman, C. Ng, S. Sinniah, X.W. Koh, N.F. Asgar, D. Li, D. Yim, et al. 2012. Structure of a novel phosphotyrosine-binding domain in Hakai that targets E-cadherin. *EMBO J.* 31:1308–1319. https://doi.org/10.1038/emboj.2011.496

Nelson, W.J., and R. Nusse. 2004. Convergence of Wnt, beta-catenin, and cadherin pathways. *Science.* 303:1483–1487. https://doi.org/10.1126/science.1094291

Omelchenko, T., J.M. Vasiliev, I.M. Gelfand, H.H. Feder, and E.M. Bonder. 2003. Rho-dependent formation of epithelial "leader" cells during wound healing. *Proc. Natl. Acad. Sci. USA.* 100:10788–10793. https://doi.org/10.1073/pnas.1834401100

Orsulic, S., O. Huber, H. Aberle, S. Arnold, and R. Kemler. 1999. E-cadherin binding prevents beta-catenin nuclear localization and beta-catenin/LEF-1-mediated transactivation. *J. Cell Sci.* 112:1237–1245.

Papkoff, J. 1997. Regulation of complexed and free catenin pools by distinct mechanisms. Differential effects of Wnt-1 and v-Src. *J. Biol. Chem.* 272:4536–4543.

Papkoff, J., and M. Aikawa. 1998. WNT-1 and HGF regulate GSK3 beta activity and beta-catenin signaling in mammary epithelial cells. *Biochem. Biophys. Res. Commun.* 247:851–858. https://doi.org/10.1006/bbrc.1998.8888

Reynolds, A.B., J. Daniel, P.D. McCrea, M.J. Wheelock, J. Wu, and Z. Zhang. 1994. Identification of a new catenin: The tyrosine kinase substrate p120cas associates with E-cadherin complexes. *Mol. Cell. Biol.* 14:8333–8342. https://doi.org/10.1128/MCB.14.12.8333

Rolland, Y., P. Marighetti, C. Malinverno, S. Confalonieri, C. Luise, N. Ducano, A. Palamidessi, S. Bisi, H. Kajiho, F. Troglio, et al. 2014. The CDC42-interacting protein 4 controls epithelial cell cohesion and tumor dissemination. *Dev. Cell.* 30:553–568. https://doi.org/10.1016/j.devcel.2014.08.006

Roura, S., S. Miravet, J. Piedra, A. García de Herreros, and M. Duñach. 1999. Regulation of E-cadherin/Catenin association by tyrosine phosphorylation. *J. Biol. Chem.* 274:36734–36740. https://doi.org/10.1074/jbc.274.51.36734

Sanson, B., P. White, and J.P. Vincent. 1996. Uncoupling cadherin-based adhesion from wingless signalling in Drosophila. *Nature.* 383:627–630. https://doi.org/10.1038/383627a0

Sarangi, B.R., M. Gupta, B.L. Doss, N. Tissot, F. Lam, R.M. Mège, N. Borghi, and B. Ladoux. 2017. Coordination between intra- and extracellular forces regulates focal adhesion dynamics. *Nano Lett.* 17:399–406. https://doi.org/10.1021/acs.nanolett.6b04364

Sawada, Y., M. Tamada, B.J. Dubin-Thaler, O. Cherniavskaya, R. Sakai, S. Tanaka, and M.P. Sheetz. 2006. Force sensing by mechanical extension of the Src family kinase substrate p130Cas. *Cell.* 127:1015–1026. https://doi.org/10.1016/j.cell.2006.09.044

Schaller, M.D. 2010. Cellular functions of FAK kinases: Insight into molecular mechanisms and novel functions. *J. Cell Sci.* 123:1007–1013. https://doi.org/10.1242/jcs.045112

Schmitz, Y., K. Rateitschak, and O. Wolkenhauer. 2013. Analysing the impact of nucleo-cytoplasmic shuttling of β-catenin and its antagonists APC, Axin and GSK3 on Wnt/β-catenin signalling. *Cell. Signal.* 25:2210–2221. https://doi.org/10.1016/j.cellsig.2013.07.005

Seong, J., M. Ouyang, T. Kim, J. Sun, P.C. Wen, S. Lu, Y. Zhuo, N.M. Llewellyn, D.D. Schlaepfer, J.L. Guan, et al. 2011. Detection of focal adhesion kinase activation at membrane microdomains by fluorescence resonance energy transfer. *Nat. Commun.* 2:406. https://doi.org/10.1038/ncomms1414

Sim, J.Y., J. Moeller, K.C. Hart, D. Ramallo, V. Vogel, A.R. Dunn, W.J. Nelson, and B.L. Pruitt. 2015. Spatial distribution of cell-cell and cell-ECM adhesions regulates force balance while maintaining E-cadherin molecular tension in cell pairs. *Mol. Biol. Cell.* 26:2456–2465.

Song, J.L., P. Nigam, S.S. Tektas, and E. Selva. 2015. microRNA regulation of Wnt signaling pathways in development and disease. *Cell. Signal.* 27:1380–1391. https://doi.org/10.1016/j.cellsig.2015.03.018

Tabdanov, E., N. Borghi, F. Brochard-Wyart, S. Dufour, and J.P. Thiery. 2009. Role of E-cadherin in membrane-cortex interaction probed by nanotube extrusion. *Biophys. J.* 96:2457–2465. https://doi.org/10.1016/j.bpj.2008.11.059

Takeda, H., A. Nagafuchi, S. Yonemura, S. Tsukita, J. Behrens, W. Birchmeier, and S. Tsukita. 1995. V-src kinase shifts the cadherin-based cell adhesion from the strong to the weak state and β catenin is not required for the shift. *J. Cell Biol.* 131:1839–1847. https://doi.org/10.1083/jcb.131.6.1839

Thiery, J.P., and J.P. Sleeman. 2006. Complex networks orchestrate epithelial-mesenchymal transitions. *Nat. Rev. Mol. Cell Biol.* 7:131–142. https://doi.org/10.1038/nrm1835

Tominaga, J., Y. Fukunaga, E. Abelardo, and A. Nagafuchi. 2008. Defining the function of beta-catenin tyrosine phosphorylation in cadherin-mediated cell-cell adhesion. *Genes Cells.* 13:67–77.

Trepat, X., et al. 2009. Physical forces during collective cell migration. *Nat. Phys.* 5:426–430. https://doi.org/10.1038/nphys1269

van Leeuwen, I.M.M., H.M. Byrne, O.E. Jensen, and J.R. King. 2007. Elucidating the interactions between the adhesive and transcriptional functions of β-catenin in normal and cancerous cells. *J. Theor. Biol.* 247:77–102. https://doi.org/10.1016/j.jtbi.2007.01.019

van Veelen, W., N.H. Le, W. Helvensteijn, L. Blonden, M. Theeuwes, E.R. Bakker, P.F. Franken, L. van Gurp, F. Meijlink, M.A. van der Valk, et al. 2011. β-catenin tyrosine 654 phosphorylation increases Wnt signalling and intestinal tumorigenesis. *Gut.* 60:1204–1212. https://doi.org/10.1136/gut.2010.233460

Wang, Y., E.L. Botvinick, Y. Zhao, M.W. Berns, S. Usami, R.Y. Tsien, and S. Chien. 2005. Visualizing the mechanical activation of Src. *Nature.* 434:1040–1045. https://doi.org/10.1038/nature03469

Weidner, K.M., J. Behrens, J. Vandekerckhove, and W. Birchmeier. 1990. Scatter factor: Molecular characteristics and effect on the invasiveness of epithelial cells. *J. Cell Biol.* 111:2097–2108. https://doi.org/10.1083/jcb.111.5.2097

Whitehead, J., D. Vignjevic, C. Fütterer, E. Beaurepaire, S. Robine, and E. Farge. 2008. Mechanical factors activate beta-catenin-dependent oncogene expression in APC mouse colon. *HFSP J.* 2:286–294. https://doi.org/10.2976/1.2955566

Zebda, N., O. Dubrovskyi, and K.G. Birukov. 2012. Focal adhesion kinase regulation of mechanotransduction and its impact on endothelial cell functions. *Microvasc. Res.* 83:71–81. https://doi.org/10.1016/j.mvr.2011.06.007

Zeng, G., U. Apte, A. Micsenyi, A. Bell, and S.P. Monga. 2006. Tyrosine residues 654 and 670 in beta-catenin are crucial in regulation of Met-beta-catenin interactions. *Exp. Cell Res.* 312:3620–3630. https://doi.org/10.1016/j.yexcr.2006.08.003

Zhou, J., C. Aponte-Santamaría, S. Sturm, J.T. Bullerjahn, A. Bronowska, and F. Gräter. 2015. Mechanism of focal adhesion kinase mechanosensing. *PLOS Comput. Biol.* 11:e1004593.